

Physics at the CLIC e^+e^- Linear Collider

Input to the Snowmass process 2013



March 10, 2022

This paper summarizes the physics potential of the CLIC high-energy e^+e^- linear collider. It provides input to the Snowmass 2013 process for the energy-frontier working groups on The Higgs Boson (HE1), Precision Study of Electroweak Interactions (HE2), Fully Understanding the Top Quark (HE3), as well as The Path Beyond the Standard Model – New Particles, Forces, and Dimensions (HE4). It is accompanied by a paper describing the CLIC accelerator study, submitted to the Frontier Capabilities group of the Snowmass process [1].

The CLIC Detector and Physics Study

H. Abramowicz¹, A. Abusleme², K. Afanaciev³, G. Alexander¹, N. Alipour Tehrani⁴, O. Alonso^{5,6}, K.K. Andersen⁷, S. Arfaoui⁴, C. Balazs^{8,9}, T. Barklow¹⁰, M. Battaglia¹¹, M. Benoit⁴, B. Bilk¹², J.-J. Blaising¹³, M. Boland^{8,14}, I. Božović Jelisavčić¹⁵, P. Burrows¹⁶, R. Contino¹⁷, D. Dannheim⁴, M. Demarteau¹², M.A. Diaz Gutierrez², A. Diéguez^{5,6}, J. Duarte Campderros^{5,18}, G. Eigen¹⁹, K. Elsener⁴, D. Feldman²⁰, U. Felzmann^{8,14}, M. Firlej²¹, E. Firtz²², T. Fiutowski²¹, K. Francis¹², F. Gaede²³, I. García García^{5,24}, V. Ghenescu²², G. Giudice⁴, N. Graf¹⁰, C. Grefe⁴, C. Grojean^{4,25}, R.S. Gupta²⁰, M. Hauschild⁴, H. Holmestad⁴, M. Idzik²¹, C. Joram⁴, S. Kananov¹, M. Killenberg^{4,23}, W. Klempt⁴, S. Kraml²⁶, B. Krupa²⁷, S. Kulis^{4,21}, T. Laštovička^{28,*}, G. LeBlanc^{8,14}, A. Levy¹, I. Levy¹, L. Linssen^{4,*}, A. Lucaci Timoce⁴, S. Lukić¹⁵, V. Makarenko³, J. Marshall²⁹, V. Martin³⁰, R.E. Mikkelsen⁷, G. Milutinovic Dumbelovic¹⁵, A. Miyamoto³¹, K. Mönig³², G. Moortgat-Pick^{23,33}, J. Moron²¹, A. Münnich^{4,23}, A. Neagu²², M. Pandurović¹⁵, D. Pappadopulo^{34,35}, B. Pawlik²⁷, W. Porod³⁶, S. Poss⁴, T. Preda²², R. Rassool^{8,37}, R. Rattazzi³⁸, S. Redford⁴, J. Repond¹², S. Riemann³², A. Robson³⁹, P. Roloff^{4,*}, E. Ros^{5,24}, J. Rosten³⁰, A. Ruiz-Jimeno^{5,18}, H. Rzehak⁴, A. Sailer^{4,*}, D. Schlatter⁴, D. Schulte⁴, F. Sefkow^{4,23}, K. Seidel⁴⁰, N. Shumeiko³, E. Sicking⁴, F. Simon^{40,*}, J. Smith¹², C. Soldner⁴⁰, S. Stapnes^{4,*}, J. Strube⁴, T. Suehara⁴¹, K. Świentek²¹, M. Szalay⁴⁰, T. Tanabe⁴², M. Tesar⁴⁰, A. Thamm^{4,38}, M. Thomson^{29,*}, J. Trenado Garcia^{5,6}, U.I. Uggerhøj⁷, E. van der Kraaij¹⁹, I. Vila^{5,18}, E. Vilella^{5,6}, M.A. Villarejo^{5,24}, M.A. Vogel Gonzalez², M. Vos^{5,24}, N. Watson⁴³, H. Weerts¹², J.D. Wells^{4,20,*}, L. Weuste⁴⁰, T.N. Wistisen⁷, K. Wootton^{8,37}, L. Xia¹², L. Zawiejski²⁷, I.-S. Zgura²²

¹ School of Physics and Astronomy, Faculty of Exact Sciences, Tel Aviv University, Tel Aviv, Israel,

² Pontificia Universidad Católica de Chile, Santiago de Chile, Chile, ³ National Scientific and Educational Centre of Particle and High Energy Physics, Belarusian State University, Minsk, Belarus,

⁴ CERN, Geneva, Switzerland, ⁵ Spanish Network for Future Linear Colliders, ⁶ Universitat de Barcelona, Barcelona, Spain, ⁷ Aarhus University, Aarhus, Denmark, ⁸ Australian Collaboration for Accelerator Science (ACAS), ⁹ Monash University, Melbourne, Australia, ¹⁰ SLAC, Stanford, USA,

¹¹ University of California, Santa Cruz, USA, ¹² Argonne National Laboratory, Argonne, USA, ¹³ Laboratoire d'Annecy-le-Vieux de Physique des Particules, Annecy-le-Vieux, France, ¹⁴ Australian Synchrotron, Clayton, Australia, ¹⁵ Vinča Institute of Nuclear Sciences, University of Belgrade, Belgrade, Serbia, ¹⁶ Oxford University, Oxford, United Kingdom, ¹⁷ Dipartimento di Fisica, Università di Roma La Sapienza, Rome, Italy, ¹⁸ IFCA, Universidad de Cantabria/CSIC, Santander, Spain,

¹⁹ Department of Physics and Technology, University of Bergen, Bergen, Norway, ²⁰ Physics Department, University of Michigan, Ann Arbor, Michigan, USA, ²¹ Faculty of Physics and Applied Computer Science, AGH University of Science and Technology, Cracow, Poland, ²² Institute of Space Science, Bucharest, Romania, ²³ DESY, Hamburg, Germany, ²⁴ IFIC, Universitat de Valencia/CSIC, Valencia, Spain, ²⁵ ICREA at IFAE, Universitat Autònoma de Barcelona, Bellaterra, Spain,

²⁶ Laboratoire de Physique Subatomique et de Cosmologie (LPSC), Université Joseph Fourier

* Corresponding Editors. Contact: clicsnow-editors@cern.ch

Grenoble 1, IN2P3/CNRS, Grenoble, France, ²⁷ The Henryk Niewodniczanski Institute of Nuclear Physics, Polish Academy of Sciences, Cracow, Poland, ²⁸ Institute of Physics of the Academy of Sciences of the Czech Republic, Prague, Czech Republic, ²⁹ University of Cambridge, Cambridge, United Kingdom, ³⁰ University of Edinburgh, Edinburgh, United Kingdom, ³¹ High Energy Accelerator Research Organization (KEK), Tsukuba, Japan, ³² DESY, Zeuthen, Germany, ³³ University of Hamburg, Hamburg, Germany, ³⁴ Department of Physics, University of California, Berkeley, USA, ³⁵ Theoretical Physics Group, Lawrence Berkeley National Laboratory, Berkeley, USA, ³⁶ Universität Würzburg, Würzburg, Germany, ³⁷ Melbourne University, Melbourne, Australia, ³⁸ Institut de Théorie des Phénomènes Physiques, Ecole Polytechnique Fédérale de Lausanne, Lausanne, Switzerland, ³⁹ University of Glasgow, Glasgow, United Kingdom, ⁴⁰ Max-Planck-Institut für Physik, Munich, Germany, ⁴¹ Department of Physics, Tohoku University, Sendai, Japan, ⁴² ICEPP, The University of Tokyo, Tokyo, Japan, ⁴³ The School of Physics and Astronomy of the University of Birmingham, Birmingham, United Kingdom

Table of Contents

1	Introduction	2
1.1	CLIC Accelerator Parameters and Options for a Staged Implementation	3
1.2	CLIC Detectors	4
1.3	CLIC Physics Optimization with Energy Staging	5
2	Higgs Physics at CLIC	8
2.1	Higgs Measurements at $\sqrt{s} = 350$ GeV	10
2.2	Higgs Measurements at $\sqrt{s} > 1$ TeV	10
2.3	Higgs Self-Coupling	13
2.4	Higgs Boson Couplings and Total Decay Width	14
2.5	Impact of the Precision Measurements of the Higgs Couplings	16
2.6	Higgs Boson Mass, Spin and CP Properties	17
3	Top Physics	18
3.1	Introduction	18
3.2	Top Quark Mass Measurements at CLIC	18
3.3	Top as a Probe for New Physics	19
3.4	Conclusion	20
4	BSM Searches	21
4.1	Introduction	21
4.2	Supersymmetry	21
4.3	Composite Higgs Boson Theories	22
4.4	Search for Exotic Physics through Direct Production and Precision Studies	23
4.5	Conclusion	24
5	Precision Study of Electroweak Interactions	27
6	Summary and Conclusions	29

1 Introduction

The Compact Linear Collider (CLIC) is a TeV scale high-luminosity linear e^+e^- collider under development. It is based on a novel two-beam acceleration technique providing acceleration gradients at the level of 100 MV/m. Recent implementation studies for CLIC have converged towards a staged approach offering a unique physics program spanning several decades. In this scheme, CLIC would provide high-luminosity e^+e^- collisions from a few hundred GeV to 3 TeV. The first stage, at or above the 350 GeV

top-pair-production threshold, gives access to precision Higgs physics through the Higgs-strahlung and WW-fusion production processes, providing absolute values of Higgs couplings to both fermions and bosons. This stage also addresses precision top physics. The second stage, around 1.4 TeV, opens the energy frontier, allowing for the discovery of New Physics phenomena. This stage also gives access to additional Higgs properties, such as the top-Yukawa coupling, the Higgs potential and rare Higgs decay branching ratios. The ultimate CLIC energy of 3 TeV enlarges the CLIC physics potential even further, covering the complete scope for precision Standard Model physics, direct searches for pair-production of new particles up to 1.5 TeV mass and optimal sensitivity to New Physics at much higher mass-scales through precision measurements. A staged implementation of CLIC along the lines described would open the door to an impressive long-term physics program at the energy frontier, beyond the LHC program. The machine is therefore considered an important option for a post-LHC facility at CERN, as emphasized in the recent update of the European Strategy for Particle Physics [2, 3].

Over the last years, the feasibility studies for the CLIC accelerator have systematically and successfully addressed the main technical challenges of the accelerator project. Similarly, detailed detector and physics studies confirm the ability to perform high-precision measurements at CLIC.

For more detailed descriptions we refer to the following documents:

- A Multi-TeV Linear Collider based on CLIC Technology, CLIC Conceptual Design Report, 2012, eds. M. Aicheler et al. [4];
- Physics and Detectors at CLIC, CLIC Conceptual Design Report, eds. L. Linssen et al. [5];
- The CLIC Programme: towards a staged e^+e^- Linear Collider exploring the Terascale, CLIC Conceptual Design Report, 2012, eds. P. Lebrun et al. [6];
- The Physics Case for an e^+e^- Linear Collider, eds. J. Brau et al., submitted to the update process of the European Strategy for Particle Physics, July 2012 [7].

The CLIC Conceptual Design Report (CDR) is supported by more than 1300 signatories¹ from the worldwide particle physics community.

1.1 CLIC Accelerator Parameters and Options for a Staged Implementation

The CLIC accelerator design is based on a novel two-beam acceleration scheme. It uses a high-intensity drive beam to generate RF power at 12 GHz. The RF is used to accelerate the main particle beam that runs in parallel to the drive beam. CLIC uses normal-conducting accelerator structures, operated at room temperature. The initial drive beams and main beams are generated in central complexes and are then injected at the end of the two-beam linac arms. The feasibility of the CLIC accelerator has been demonstrated through prototyping, simulations and large-scale tests, as described in the conceptual design report [4]. In particular, the two-beam acceleration at gradients exceeding 100 MV/m has been demonstrated in the CLIC test facility CTF3. High luminosities are achieved by very small beam emittances, which are generated in the injector complex and maintained during transport to the interaction point.

The CLIC accelerator can be built in energy stages, re-using the existing equipment for each new stage. At each energy stage the center-of-mass energy can be tuned to lower values within a range of approximately a factor three with limited loss in luminosity performance. The ultimate choice of the CLIC energy stages will be driven by the physics aims, where further input from LHC data, in particular 14 TeV data, is expected. The recent LHC Higgs discovery makes an initial energy stage around 350 GeV to 375 GeV very attractive, but final choices will depend on further LHC findings. In the first stage around 350 GeV and second stage around 1.4 TeV a single drive-beam generation complex feeds both linacs, while in the third stage at 3 TeV each linac is fed by a separate complex. The accelerator parameters

¹<https://edms.cern.ch/document/1183227/>

Table 1: Center-of-mass energy and assumed integrated luminosity for the different CLIC machine stages. The integrated luminosities correspond each to four or five years of operation of a fully commissioned machine running 200 days per year with an effective up-time of 50%.

Parameter	Symbol	Unit	Stage 1	Stage 2	Stage 3
Center-of-mass energy	\sqrt{s}	GeV	350	1400	3000
Integrated luminosity	\mathcal{L}_{int}	ab^{-1}	0.5	1.5	2.0

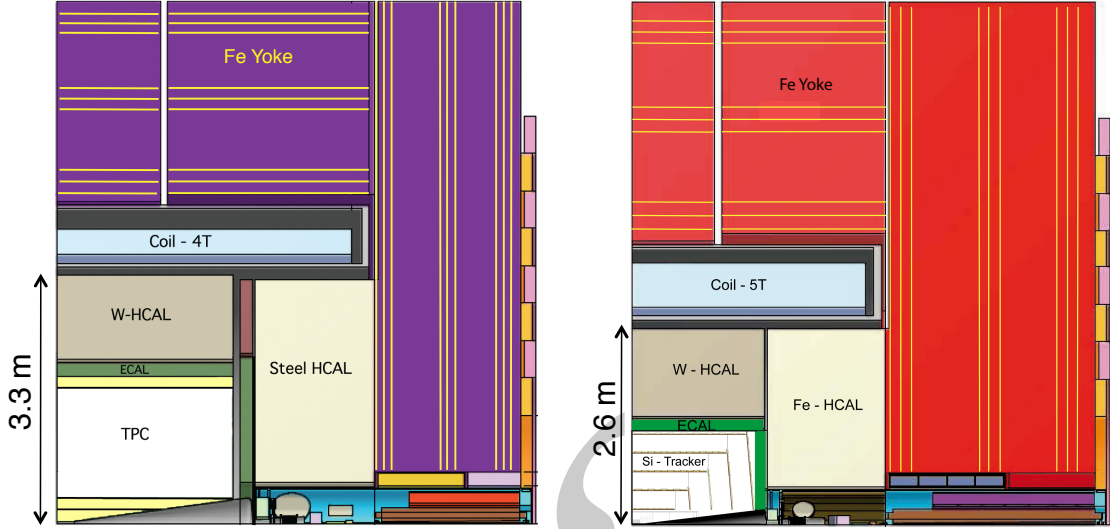


Fig. 1: Longitudinal cross section of the top right quadrant of CLIC_ILD (left) and CLIC_SiD (right).

are based on detailed accelerator studies, described in the CDR [4], and are used for the physics studies presented in this paper. The assumed integrated luminosities of 0.5 ab^{-1} at 350 GeV, 1.5 ab^{-1} at 1.4 TeV, and 2.0 ab^{-1} at 3 TeV correspond each to four or five years of operation of a fully commissioned machine running 200 days per year with an effective up-time of 50% (Table 1). The CLIC design foresees 80% electron polarization, while space is reserved in the layout for a positron polarization option.

Motivated by the discovery of the 125 GeV Higgs boson, studies for a klystron-based initial stage at 375 GeV are currently being carried out. This option could provide a faster implementation, while still allowing for the re-use of equipment at the higher energy stages.

1.2 CLIC Detectors

The detector concepts used for the CLIC physics studies are based on the SiD [8] and ILD [9] detector concepts for the International Linear Collider. They were adapted for the CLIC 3 TeV accelerator stage, which constitutes the most challenging environment for the detectors. In a staged scenario, most sub-detectors will serve at all center-of-mass energies, while e.g., the inner tracking and vertex detectors would profit from a version with a smaller inner radius at the lower energies.

1.2.1 Detector Performance Requirements and Detector Concepts

The performance requirements for the CLIC detectors are given by the physics goals. They are:

- Jet energy resolution of $\sigma_E/E \lesssim 3.5\%$ for jet energies from 100 GeV to 1 TeV ($\lesssim 5\%$ at 50 GeV);
- Track momentum resolution of $\sigma_{p_T}/p_T^2 \lesssim 2 \cdot 10^{-5} \text{ GeV}^{-1}$;

- Impact parameter resolution of $\sigma_{d_0}^2 = (5 \mu\text{m})^2 + (15 \mu\text{m})^2/p^2 \sin^3 \theta$;
- Lepton identification efficiency better than 95% over the full range of energies;
- Detector coverage for electrons down to very low angles.

The jet energy resolution is required to distinguish W, Z, or H bosons, for example, to study the decay chains of charginos and neutralinos. The momentum resolution is driven, for example, by the muon momentum measurement in HZ recoil events or for measuring the Higgs decay to muons. It is also motivated by, for example, slepton mass measurements. Efficient vertex reconstruction and flavor tagging is needed, for example for the measurement of Higgs branching ratios to beauty or charm. The full coverage is important to suppress Standard Model backgrounds in various physics analyses. In particular, many physics background processes involve electrons in the forward region.

Vertical cuts through the top-right quadrant of CLIC_ILD (left) and CLIC_SiD (right) are shown in [Figure 1](#). The jet energy resolution requirement is the main driver of the detector concept designs. As a result both detector concepts are based on fine-grained calorimeters and optimized for particle-flow analysis techniques. In the particle-flow approach all visible particles are reconstructed by combining the information from precise tracking with highly granular calorimetry. The technique achieves an optimal jet energy resolution through the separation of individual particles within the jet [10, 11]. The detectors comprise strong central solenoid magnets, with a field of 5 T in CLIC_SiD and 4 T in CLIC_ILD. The tracking system of CLIC_SiD is fully based on silicon pixel and strip detectors, while the tracker of CLIC_ILD combines silicon pixels with silicon strips and a large Time Projection Chamber.

CLIC beams will arrive at the detector in bunch trains, occurring every 20 ns. Each bunch train generates 312 bunch crossings at 0.5 ns time separation (3 TeV values). This time structure allows for a trigger-less readout of the detectors after each bunch train. It also allows for a power-pulsing scheme of the on-detector electronics, thereby significantly reducing the power dissipation and the tracker mass. On average less than one physics event per bunch train is expected. However, the high CLIC energies and small intense beams lead to significant beamstrahlung, resulting in high rates of incoherent electron-positron pairs and $\gamma\gamma \rightarrow \text{hadron}$ events. The energy loss through beamstrahlung also generates a tail to the luminosity spectrum that extends well below the nominal center-of-mass energy.

Even at 3 TeV, the impact of beam-induced backgrounds can be reduced by making use of the high spatial and temporal granularity provided by the detectors. The method relies on precise hit timing (10 ns time-stamping for all silicon tracking elements and 1 ns hit time resolution for all calorimeter hits) combined with offline event reconstruction, including the background particles, with particle flow analysis. With a tight set of cuts applied to the reconstructed low- p_T particles, the average background level can be reduced from approximately 20 TeV per bunch train to about 100 GeV per reconstructed physics event. This background rejection, which is exemplified in [Figure 2](#), is achieved without significantly impacting the physics performance. The remaining background particles can be further rejected by applying hadron-collider type jet clustering algorithms, which treat the very forward particles similar to the underlying event in hadronic collisions.

The CLIC CDR studies have demonstrated that the requirements for high-precision physics measurements under CLIC experimental conditions can be fulfilled. This is illustrated in more detail in the following sections.

1.3 CLIC Physics Optimization with Energy Staging

The main asset and aim of the CLIC acceleration technology is to provide scope for exploring New Physics at multi-TeV e^+e^- center-of-mass energies and with very high luminosities. Until now it is the only technology option on the market that can reach such high energies and for which the feasibility has been demonstrated in large-scale test facilities and at the level of the design parameters required

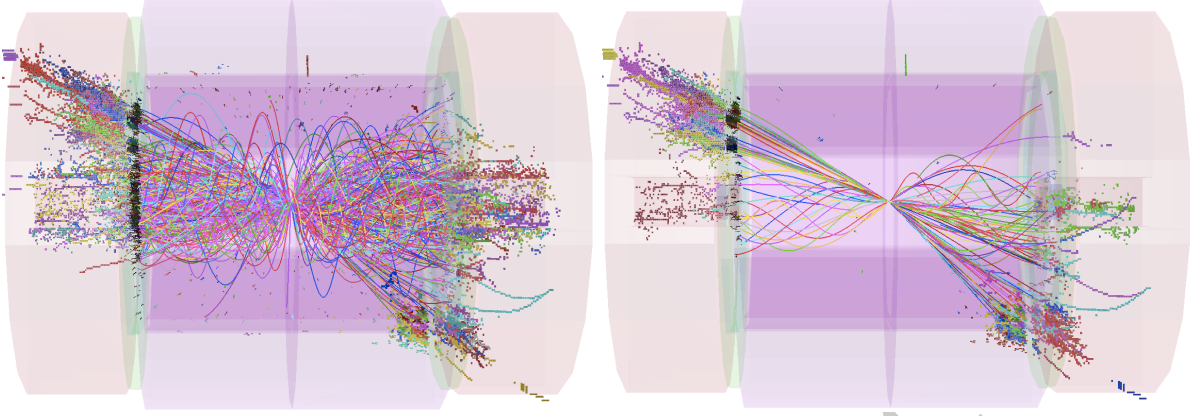


Fig. 2: Left: Reconstructed particles in a simulated $e^+e^- \rightarrow t\bar{t}$ event at 3 TeV in the CLIC_ILD detector concept with background from $\gamma\gamma \rightarrow \text{hadrons}$ overlaid in a broad reconstruction window around the physics event. Right: The effect of applying tight timing cuts on the reconstructed particles.

for the complete facility, as detailed in the conceptual design report [4]. The CLIC technique requires large investments in its injector complex, while offering a relatively modest marginal cost per GeV for the acceleration linac [6]. CLIC is therefore principally justified as an exploration machine for New Physics at the high-energy frontier. The full physics potential of CLIC, however, also includes known SM physics, with highly relevant topics like precision Higgs and top physics to be studied from \sqrt{s} of a few hundred GeV onwards. New Physics could already show up at the scale of a few hundred GeV, as e^+e^- collisions may give access to states, e.g., electroweak particles, that could remain undetected in proton-proton collisions at the LHC. At increasing \sqrt{s} , additional Higgs production and decay channels become accessible, while the window for New Physics opens up more and more.

Cross sections for many of the interesting phenomena are low, at the fb level, therefore high integrated luminosities are essential all along the CLIC energy range. By constructing and operating the machine in a few energy stages the luminosity performance over the full CLIC energy range can be maximized, without compromising the re-use of equipment from the earlier stages at the higher energies. At each stage the energy can be tuned down within a range of a factor ≈ 3 with limited luminosity performance loss.

Final choices for the CLIC energy stages will depend on the physics results from LHC running at 14 TeV. For illustration, a possible staging scenario can be inferred from Figure 3, showing cross sections for Higgs and top production and for a possible SUSY scenario as a function of the center-of-mass energy. A first CLIC energy stage around 350 GeV to 375 GeV is very well motivated by Higgs and top physics. A next energy stage, around ≈ 1.4 TeV, would give access to the detection and precise measurements of gauginos and sleptons in the example SUSY model (labelled *model III* [6]), while also providing additional Higgs precision measurements through vector-boson fusion, $t\bar{t}H$ production and double-Higgs production. A third stage at the highest CLIC energy of 3 TeV would complement precision Higgs physics, e.g., for decays with very small branching ratios, while also giving access to heavy Higgs partners and squarks in the example SUSY scenario.

In the following sections, the CLIC physics capabilities with this staging scenario are elaborated in more detail. Section 2 describes the potential for precision Higgs physics and its impact on our knowledge of the underlying EWSB process and of New Physics scenarios. Section 3 gives an overview of top physics at CLIC. The section puts emphasis on top mass measurements, and illustrates other examples of top physics at CLIC, which will be studied in more detail in the near future. Section 4 illustrates the CLIC potential for physics searches beyond the standard model. Precision measurements are mostly already included in the Higgs, top and BSM sections, and are summarized together in Section 5. Overall

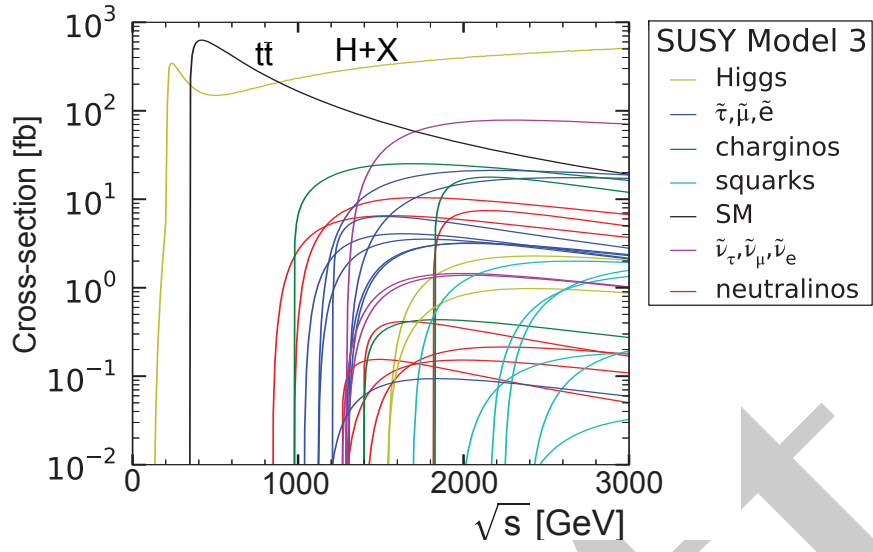


Fig. 3: Higgs, $t\bar{t}$ and SUSY production cross sections of *model III* as a function of \sqrt{s} . Every line of a given color corresponds to the production cross section of one particle in the legend.

conclusions and an outlook are presented in [Section 6](#).

2 Higgs Physics at CLIC

A high-energy e^+e^- collider such as CLIC would provide a clean environment to study the properties of the Higgs boson with very high precision. The different CLIC energy stages will enable measurements of the properties of a 125 GeV Standard Model like Higgs boson through a number of different production processes, where those with the highest cross sections are indicated in [Figure 4](#). The sensitivities to Higgs physics at CLIC have been studied in the context of the staged scenario described previously. The results from these studies have been obtained using detailed GEANT4 detector simulations, full reconstruction with the dominant background from $\gamma\gamma \rightarrow \text{hadrons}$ overlaid and inclusion of all relevant Standard Model background processes.

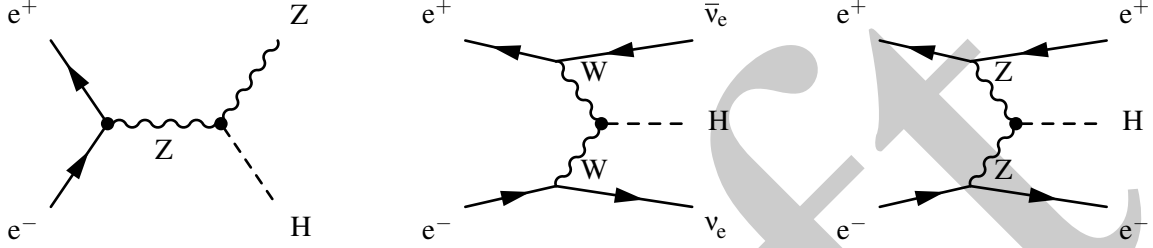


Fig. 4: The three highest cross section Higgs production processes at CLIC. At $\sqrt{s} \approx 350$ GeV, the Higgs-strahlung process dominates. Above $\sqrt{s} \approx 500$ GeV, the WW vector boson fusion process $e^+e^- \rightarrow H\nu_e\bar{\nu}_e$ is dominant, with the cross section for the ZZ process being about one order of magnitude lower.

In the initial stage of CLIC operation at $\sqrt{s} \approx 350$ GeV, the Higgs-strahlung process $e^+e^- \rightarrow ZH$ dominates, allowing a precise model-independent measurement of the coupling of the Higgs boson to the Z and providing precise measurements of the Higgs boson branching ratios to a number of final states. In the higher energy stages of CLIC operation (1.4 TeV and 3.0 TeV), large samples of Higgs bosons will be produced primarily through the vector boson fusion process, $e^+e^- \rightarrow H\nu_e\bar{\nu}_e$. These large data samples will allow very precise $\mathcal{O}(1\%)$ measurements of the couplings of the Higgs boson to both fermions and the gauge bosons. In addition to the main Higgs production processes, rarer processes such as $e^+e^- \rightarrow t\bar{t}H$ and $e^+e^- \rightarrow HH\nu_e\bar{\nu}_e$, shown in [Figure 5](#), provide access to the top quark Yukawa coupling and the Higgs trilinear self-coupling as determined by the parameter λ in the Higgs potential.

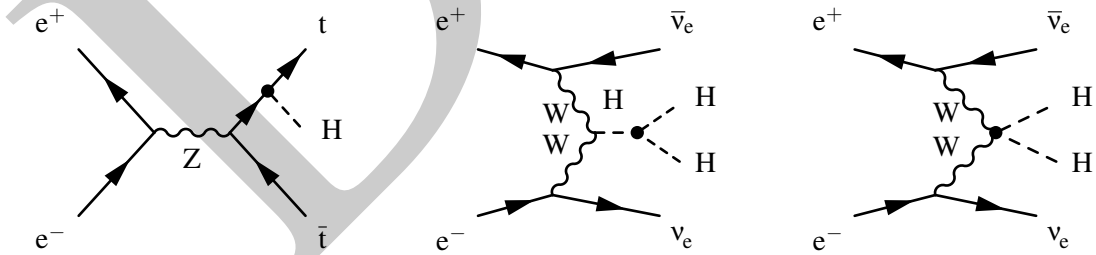


Fig. 5: The main processes at CLIC involving the top-quark Yukawa coupling g_{Htt} , the Higgs boson trilinear self-coupling λ and the quartic coupling g_{HHWW} .

The raw Higgs production cross sections as a function of center-of-mass energy are shown in [Figure 6](#). The relatively large Higgs production cross sections, combined with the high integrated luminosities achievable at CLIC, result in large samples of Higgs bosons (far surpassing the number of W bosons produced at LEP). [Table 2](#) compares the expected number of ZH and $H\nu_e\bar{\nu}_e$ events at the three main center-of-mass energies considered in a CLIC energy staged scenario. The numbers of events include the effect of beamstrahlung, which results in a tail in the distribution of the effective center-of-mass energy $\sqrt{s'}$. Even at the lowest CLIC energies considered here, large and clean samples of Higgs boson decays

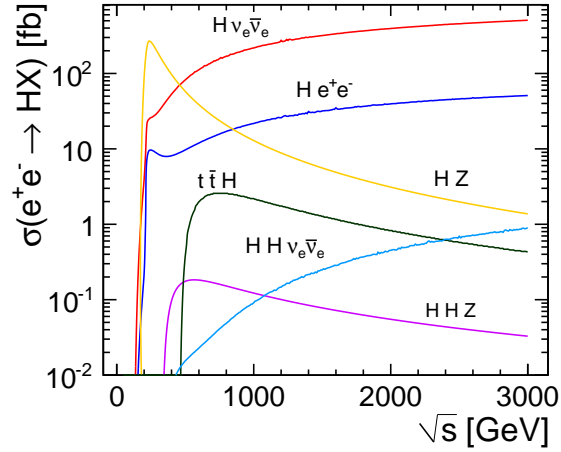


Fig. 6: The center-of-mass dependencies of the cross sections for the main Higgs production processes at an e^+e^- collider. The values shown correspond to unpolarized beams and do not include the effects of initial-state radiation (ISR) or beamstrahlung.

Table 2: The leading-order Higgs *unpolarized* cross sections for the Higgs-strahlung, WW-fusion, and ZZ-fusion processes for $m_H = 125$ GeV at the three center-of-mass energies discussed in this document. The quoted cross sections include the effects of ISR but do not include the effects of beamstrahlung. Also listed are the numbers of expected events *including* the effects of beamstrahlung and ISR. The impact of beamstrahlung on the expected numbers of events is relatively small, leading to an approximately 10% reduction in the numbers of $H\nu_e\bar{\nu}_e$ events at $\sqrt{s} > 1$ TeV. The cross sections and expected numbers do not account for the enhancements possible from polarized beams.

	350 GeV	1.4 TeV	3 TeV
\mathcal{L}_{int}	500 fb ⁻¹	1500 fb ⁻¹	2000 fb ⁻¹
$\sigma(e^+e^- \rightarrow ZH)$	134 fb	9 fb	2 fb
$\sigma(e^+e^- \rightarrow H\nu_e\bar{\nu}_e)$	52 fb	279 fb	479 fb
$\sigma(e^+e^- \rightarrow He^+e^-)$	7 fb	28 fb	49 fb
# ZH events	68,000	20,000	11,000
# $H\nu_e\bar{\nu}_e$ events	26,000	370,000	830,000
# He^+e^- events	3,700	37,000	84,000

can be accumulated. The ZZ fusion process $e^+e^- \rightarrow He^+e^-$ has a cross section that is approximately an order of magnitude smaller than the WW fusion process, is also a significant source of Higgs bosons.

The measurement of the absolute coupling of the Higgs boson to the Z, which can be obtained from the recoil mass distribution in $HZ \rightarrow He^+e^-$ and $HZ \rightarrow H\mu^+\mu^-$ (see [Section 2.1](#)), plays a central role in the determination of the absolute Higgs couplings at a linear collider. For this reason, it might seem surprising that no significant running is considered at $\sqrt{s} = 250$ GeV, which is close to the maximum of the Higgs-strahlung cross section (see [Figure 6](#)). However, the reduction in cross section is, in part, compensated by the increased instantaneous luminosity achievable at a higher center-of-mass energy; the instantaneous luminosity is expected to approximately linearly scale with the center-of-mass energy. For this reason the precision on the coupling g_{HZZ} at 350 GeV is comparable to that achievable at 250 GeV for the same period of operation, as indicated in [Table 3](#). Furthermore, for the majority of final states, the measurement $\sigma(HZ) \times BR(H \rightarrow X)$ would be slightly more precise at $\sqrt{s} = 350$ GeV. Initial operation at $\sqrt{s} \approx 350$ GeV also allows access to Higgs production through the WW fusion process, providing

Table 3: Precision measurements of the Higgs coupling to the Z at $\sqrt{s} = 250$ GeV and $\sqrt{s} = 350$ GeV based on full simulation studies with $m_H = 120$ GeV. Results from [12] and follow-up studies [13]. The numbers assume that the accelerator, in this case the ILC, operates with $-80\%, +30\%$ electron and positron beam polarizations.

\sqrt{s}	250 GeV	350 GeV	350 GeV
\mathcal{L}_{int}	250 fb $^{-1}$	350 fb $^{-1}$	500 fb $^{-1}$
$\Delta(\sigma)/\sigma$	3%	3.7%	3.1%
$\Delta(g_{\text{HZZ}})/g_{\text{HZZ}}$	1.5%	1.9%	1.6%

a constraint on the Higgs coupling to the W boson. In addition, operation at $\sqrt{s} \approx 350$ GeV enables detailed studies of the top-pair production process. For these reasons, $\sqrt{s} \approx 350$ GeV is the preferred option for the first stage of CLIC operation and no running at $\sqrt{s} \approx 250$ GeV is currently foreseen.

2.1 Higgs Measurements at $\sqrt{s} = 350$ GeV

The Higgs-strahlung process provides the opportunity to study the couplings of the Higgs boson in a *model-independent* manner. This is unique to an electron-positron collider. The clean experimental environment, and the relatively low SM cross sections for background processes, allow $e^+e^- \rightarrow \text{ZH}$ events to be selected based solely on the identification of two opposite charged leptons with an invariant mass consistent with m_Z . The remainder of the event, the particles from the Higgs decay, is not considered in the event selection. For example, Figure 7 shows the simulated invariant mass distribution of the system recoiling against identified $Z \rightarrow \mu^+\mu^-$ decays at CLIC for $\sqrt{s} = 350$ GeV. A clear peak at the generated Higgs mass of $m_H = 125$ GeV is observed. Because only the properties of the di-lepton system are used in the selection, this method provides an absolute measurement of the Higgs-strahlung cross section, regardless of the Higgs boson decay modes; it would be equally valid if the Higgs boson decayed to invisible final states. Hence a model-independent measurement of the coupling g_{HZZ} can be made. With a dedicated analysis using also the hadronic decays of the Z, the sensitivity to invisible decay modes can be improved significantly as compared to the fully model-independent analysis. An e^+e^- linear collider provides unique sensitivity to invisible decay modes of the Higgs boson, extending down to a branching ratio into invisible states as low as 1%. For unpolarized beams, the study of the simulated ZH recoil mass distributions for $Z \rightarrow e^+e^-$ and $Z \rightarrow \mu^+\mu^-$ decays at CLIC operating at $\sqrt{s} = 350$ GeV, gives a precision on the Higgs-strahlung cross section of approximately 4% [6] for $m_H = 125$ GeV.

The recoil mass study provides an absolute measurement of the total ZH production cross section, and therefore the total number of Higgs bosons produced would be known with a statistical precision of about 4%. The systematic uncertainties from the knowledge of the integrated luminosity and event selection are expected to be significantly smaller. Subsequently, by identifying the individual final states for different Higgs and Z decay modes, measurements of the Higgs boson branching fractions can be made. Because of the high flavor-tagging efficiencies [5] achievable at CLIC, the $H \rightarrow b\bar{b}$ and $H \rightarrow c\bar{c}$ decays can be cleanly separated. Neglecting the Higgs decays into light quarks, one can also infer the branching ratio of $H \rightarrow g\bar{g}$. Table 4 summarizes the branching fraction precisions achievable at CLIC operating at 350 GeV. This table also lists the measurement sensitivities achievable at CLIC operating above 1 TeV.

2.2 Higgs Measurements at $\sqrt{s} > 1$ TeV

The large samples of events from both WW and ZZ fusion processes that could be accumulated above a center-of-mass energy of 1 TeV would lead to a measurement of the relative couplings of the Higgs boson to the W and Z bosons at the $\mathcal{O}(1\%)$ level, providing a strong test of the Standard Model prediction for

Table 4: The precisions obtainable for the Higgs observables at CLIC for integrated luminosities of 500 fb^{-1} at $\sqrt{s} = 350 \text{ GeV}$, 1.5 ab^{-1} at $\sqrt{s} = 1.4 \text{ TeV}$, and 2.0 ab^{-1} at $\sqrt{s} = 3.0 \text{ TeV}$. In all cases unpolarized beams have been assumed. The majority of the results are from the full detector simulation and reconstruction including overlaid background from $\gamma\gamma \rightarrow \text{hadrons}$. The numbers marked by ‘*’ are preliminary and the numbers marked by ‘†’ are estimates; these will be updated when full simulation results are available. The ‘—’ indicates that a measurement is not possible or relevant at this center-of-mass energy and ‘tbd’ indicates that no results or estimates are yet available. For the branching ratios, the measurement precision refers to the expected statistical uncertainty on the product of the relevant cross section and branching ratio; this is *equivalent* to the expected statistical uncertainty of the product of couplings and Γ_H . For the measurements from the $t\bar{t}H$ and $HH\nu_e\bar{\nu}_e$ processes, the measurement precisions give the expected statistical uncertainties on the quantity or quantities listed under the observable heading.

Channel	Measurement	Observable	Statistical precision		
			350 GeV 500 fb ⁻¹	1.4 TeV 1.5 ab ⁻¹	3.0 TeV 2.0 ab ⁻¹
ZH	Recoil mass distribution	m_H	120 MeV	—	—
ZH	$\sigma(\text{HZ}) \times BR(H \rightarrow \text{invisible})$	Γ_{inv}	tbd	—	—
ZH	$H \rightarrow b\bar{b}$ mass distribution	m_H	tbd	—	—
$H\nu_e\bar{\nu}_e$	$H \rightarrow b\bar{b}$ mass distribution	m_H	—	40 MeV*	33 MeV*
ZH	$\sigma(\text{HZ}) \times BR(Z \rightarrow \ell^+\ell^-)$	g_{HZZ}^2	4.2%	—	—
ZH	$\sigma(\text{HZ}) \times BR(H \rightarrow b\bar{b})$	$g_{\text{HZZ}}^2 g_{\text{Hbb}}^2 / \Gamma_H$	1% [†]	—	—
ZH	$\sigma(\text{HZ}) \times BR(H \rightarrow c\bar{c})$	$g_{\text{HZZ}}^2 g_{\text{Hcc}}^2 / \Gamma_H$	5% [†]	—	—
ZH	$\sigma(\text{HZ}) \times BR(H \rightarrow g\bar{g})$		6% [†]	—	—
ZH	$\sigma(\text{HZ}) \times BR(H \rightarrow \tau^+\tau^-)$	$g_{\text{HZZ}}^2 g_{\text{H}\tau\tau}^2 / \Gamma_H$	5.7%	—	—
ZH	$\sigma(\text{HZ}) \times BR(H \rightarrow WW^*)$	$g_{\text{HZZ}}^2 g_{\text{HWW}}^2 / \Gamma_H$	2% [†]	—	—
ZH	$\sigma(\text{HZ}) \times BR(H \rightarrow ZZ^*)$	$g_{\text{HZZ}}^2 g_{\text{HZZ}}^2 / \Gamma_H$	tbd	—	—
$H\nu_e\bar{\nu}_e$	$\sigma(H\nu_e\bar{\nu}_e) \times BR(H \rightarrow b\bar{b})$	$g_{\text{HWW}}^2 g_{\text{Hbb}}^2 / \Gamma_H$	3% [†]	0.3%	0.2%
$H\nu_e\bar{\nu}_e$	$\sigma(H\nu_e\bar{\nu}_e) \times BR(H \rightarrow c\bar{c})$	$g_{\text{HWW}}^2 g_{\text{Hcc}}^2 / \Gamma_H$	—	2.9%	2.7%
$H\nu_e\bar{\nu}_e$	$\sigma(H\nu_e\bar{\nu}_e) \times BR(H \rightarrow g\bar{g})$		—	1.8%	1.8%
$H\nu_e\bar{\nu}_e$	$\sigma(H\nu_e\bar{\nu}_e) \times BR(H \rightarrow \tau^+\tau^-)$	$g_{\text{HWW}}^2 g_{\text{H}\tau\tau}^2 / \Gamma_H$	—	3.7%	tbd
$H\nu_e\bar{\nu}_e$	$\sigma(H\nu_e\bar{\nu}_e) \times BR(H \rightarrow \mu^+\mu^-)$	$g_{\text{HWW}}^2 g_{\text{H}\mu\mu}^2 / \Gamma_H$	—	28%*	16%
$H\nu_e\bar{\nu}_e$	$\sigma(H\nu_e\bar{\nu}_e) \times BR(H \rightarrow \gamma\gamma)$		—	15%*	tbd
$H\nu_e\bar{\nu}_e$	$\sigma(H\nu_e\bar{\nu}_e) \times BR(H \rightarrow Z\gamma)$		—	tbd	tbd
$H\nu_e\bar{\nu}_e$	$\sigma(H\nu_e\bar{\nu}_e) \times BR(H \rightarrow WW^*)$	$g_{\text{HWW}}^4 / \Gamma_H$	tbd	1% [†]	0.7% [†]
$H\nu_e\bar{\nu}_e$	$\sigma(H\nu_e\bar{\nu}_e) \times BR(H \rightarrow ZZ^*)$	$g_{\text{HWW}}^2 g_{\text{HZZ}}^2 / \Gamma_H$	—	3% [†]	2% [†]
He^+e^-	$\sigma(\text{He}^+e^-) \times BR(H \rightarrow b\bar{b})$	$g_{\text{HZZ}}^2 g_{\text{Hbb}}^2 / \Gamma_H$	—	1% [†]	0.7% [†]
$t\bar{t}H$	$\sigma(t\bar{t}H) \times BR(H \rightarrow b\bar{b})$	$g_{\text{H}t\bar{t}}^2 g_{\text{Hbb}}^2 / \Gamma_H$	—	8% [†]	tbd
$HH\nu_e\bar{\nu}_e$	$\sigma(HH\nu_e\bar{\nu}_e)$	g_{HHWW}	—	7%*	3%*
$HH\nu_e\bar{\nu}_e$	$\sigma(HH\nu_e\bar{\nu}_e)$	λ	—	28%	16%
$HH\nu_e\bar{\nu}_e$	with -80% e^- polarization	λ	—	21%	12%

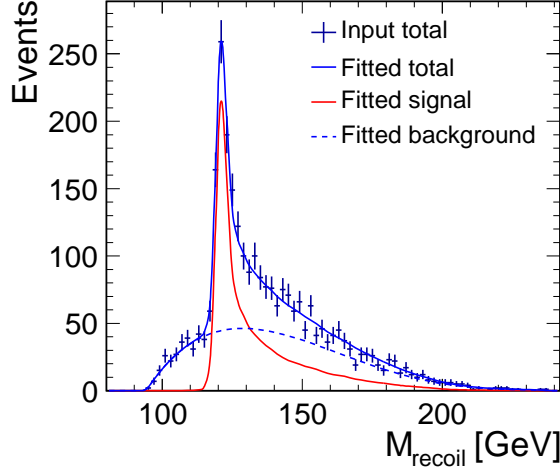


Fig. 7: The recoil mass distribution for $e^+e^- \rightarrow ZH \rightarrow \mu^+\mu^-H$ events with $m_H = 125$ GeV in the CLIC_ILD detector concept [6]. The numbers of events correspond to 500 fb^{-1} at $\sqrt{s} = 350$ GeV, and the error bars show the expected statistical uncertainties on the individual points.

$$g_{HWW}/g_{HZZ} = \cos^2 \theta_W.$$

In addition, the ability for clean flavor tagging combined with the large samples of WW fusion events allows the production rate of $e^+e^- \rightarrow H\nu_e\bar{\nu}_e \rightarrow b\bar{b}\nu_e\bar{\nu}_e$ to be determined with a statistical precision of much better than 1%. In general, the Higgs production cross section multiplied by the appropriate Higgs boson decay branching ratios can be measured more precisely at high energies, as can be seen from [Table 4](#). The uncertainties of the Higgs boson couplings to fermions and gauge bosons can be obtained by combining the high-energy CLIC results with those from the Higgs-strahlung process at $\sqrt{s} = 350$ GeV. Furthermore, the high statistics samples from the $e^+e^- \rightarrow H\nu_e\bar{\nu}_e$ alone would provide precise measurements of *relative* Higgs branching ratios. For example, CLIC operating at 3 TeV would yield a statistical precision of 1.5% on the ratio g_{Hcc}/g_{Hbb} , providing a direct comparison of the Standard Model coupling predictions for up-type (charge +2/3) and down-type (charge -1/3) quarks.

Finally, CLIC operation at $\sqrt{s} = 1.4$ TeV and above enables a determination of the top Yukawa coupling from the process $e^+e^- \rightarrow t\bar{t}H \rightarrow bW^+\bar{b}W^-H$. This process has been studied for the cases where the Higgs boson decays to $b\bar{b}$ and W^+W^- decays either fully hadronically ($q\bar{q}q\bar{q}$) or semi-leptonically ($q\bar{q}\ell\nu$). Despite the complex final states of six or eight jets, it has been shown that the top Yukawa coupling can be measured with a precision of about 4%.

2.2.1 Impact of Beam Polarization

To date, all CLIC Higgs physics studies were performed assuming unpolarized e^+ and e^- beams. However, for CLIC the baseline electron polarization is $\pm 80\%$ and there is the possibility of positron polarization at a lower level. For an electron polarization of P_- and positron polarization of P_+ , the relative fractions of collisions in the different polarization states are

$$\begin{aligned} e_R^- e_R^+ &: \frac{1}{4}(1+P_-)(1+P_+) & e_R^- e_L^+ &: \frac{1}{4}(1+P_-)(1-P_+) \\ e_L^- e_R^+ &: \frac{1}{4}(1-P_-)(1+P_+) & e_L^- e_L^+ &: \frac{1}{4}(1-P_-)(1-P_+). \end{aligned}$$

Consequently, the s -channel $e^+e^- \rightarrow ZH$ process and, in particular, the t -channel $e^+e^- \rightarrow H\nu_e\bar{\nu}_e$ process can be enhanced by beam polarization, as indicated in [Table 5](#). The chiral nature of the weak coupling

Table 5: Increases in the event rates for the s -channel $e^+e^- \rightarrow ZH$ and the t -channel $e^+e^- \rightarrow H\nu_e\bar{\nu}_e$ processes for three example beam polarizations.

Polarization $P(e^-) : P(e^+)$	Enhancement factor	
	$e^+e^- \rightarrow ZH$	$e^+e^- \rightarrow H\nu_e\bar{\nu}_e$
unpolarized	1.00	1.00
−80% : 0%	1.13	1.80
−80% : +30%	1.41	2.34

to fermions results in significant possible enhancements in the WW-fusion Higgs production mechanism. The results listed in Table 4 assume no beam polarization, although significant improvements in precision could be obtained if one were to assume −80% (left-handed) electron beam polarization (and possible additional positron polarization). In practice, the balance between operation with different beam polarizations will depend on the CLIC physics program taken as a whole.

2.3 Higgs Self-Coupling

In the SM, the Higgs boson originates from a doublet of complex scalar fields described by the potential

$$V(\phi) = \mu^2 \phi^\dagger \phi + \lambda (\phi^\dagger \phi)^2.$$

After spontaneous symmetry breaking, this form of the potential gives rise to a trilinear Higgs self-coupling of strength proportional to λv , where v is the vacuum expectation value of the Higgs potential. The measurement of the strength of the Higgs self-coupling therefore provides direct access to the quartic potential coupling λ assumed in the Higgs mechanism. This measurement is therefore an essential part of experimentally establishing the Higgs mechanism as described by the Standard Model. For $m_H = 125$ GeV, the measurement of the Higgs boson self-coupling at the LHC will be extremely challenging even with 3000 fb^{-1} of data.

At a linear collider, the trilinear Higgs coupling can be measured through the $e^+e^- \rightarrow ZHH$ and $e^+e^- \rightarrow HH\nu_e\bar{\nu}_e$ processes. The achievable precision has been studied for the $e^+e^- \rightarrow ZHH$ process at $\sqrt{s} = 500$ GeV in the context of the International Linear Collider (ILC), where the results show that a very large integrated luminosity is required [14]. For this reason, the most favourable channel for the measurement of the Higgs self-coupling is the $e^+e^- \rightarrow HH\nu_e\bar{\nu}_e$ process at $\sqrt{s} \geq 1$ TeV. Here the sensitivity increases with increasing center-of-mass energy and results from a detailed study indicate that a precision of 28% and 16% on λ could be achieved at CLIC operating respectively at $\sqrt{s} = 1.4$ TeV and $\sqrt{s} = 3$ TeV, see Table 4. These preliminary studies were performed assuming unpolarized beams. With 80% left-handed polarized electrons and 30% right-handed polarized positrons the signal cross section increases significantly and a measurement precision of $\approx 10\%$ on λ is attainable with CLIC operation at $\sqrt{s} = 3$ TeV.

The $e^+e^- \rightarrow HH\nu_e\bar{\nu}_e$ process can proceed through several lowest-order Feynman diagrams. The diagram involving the coupling λ is shown in Figure 5 (center). The expected precision on λ quoted above assumes that the contributions to the production cross section from other diagrams take their Standard Model values. However, the analysis of the process $e^+e^- \rightarrow HH\nu_e\bar{\nu}_e$ can be interpreted differently, for example as measurement of the quartic coupling at the HHWW vertex, where the sensitivity comes from the Feynman diagram shown in Figure 5 (right). A preliminary study indicates that measurement precisions of 7% and 3% on g_{HHWW} can be achieved at CLIC operating respectively at $\sqrt{s} = 1.4$ TeV and $\sqrt{s} = 3$ TeV.

2.4 Higgs Boson Couplings and Total Decay Width

In the previous sections, the Higgs boson measurements at CLIC were reviewed. In most cases the measurements correspond to the product of the Higgs production cross section with the relevant Higgs branching ratio. The absolute couplings of the Higgs boson can be determined using the total $e^+e^- \rightarrow ZH$ cross section from the recoil mass distribution from $Z \rightarrow e^-e^+$ and, in particular, $Z \rightarrow \mu^+\mu^-$, measured at $\sqrt{s} = 350$ GeV. This allows the coupling of the Higgs boson to the Z to be determined with a precision of about 2% in a model-independent manner. Once the coupling to the Z is known, the Higgs coupling to the W can be determined from, for example, the ratios of Higgs-strahlung to WW fusion cross sections,

$$\frac{\sigma(e^+e^- \rightarrow ZH) \times BR(H \rightarrow b\bar{b})}{\sigma(e^+e^- \rightarrow \nu_e\bar{\nu}_e H) \times BR(H \rightarrow b\bar{b})} \propto \left(\frac{g_{HZZ}}{g_{HWW}} \right)^2.$$

In order to determine absolute measurements of the other Higgs couplings, the Higgs total decay width needs to be inferred from the data. For a Higgs boson mass of 125 GeV, the total Higgs decay width in the SM (Γ_H) is less than 5 MeV and cannot be measured directly. However, given that the absolute couplings of the Higgs boson to the Z and W can be obtained as described above, the total decay width of the Higgs boson can be determined from $H \rightarrow WW^*$ or $H \rightarrow ZZ^*$ decays. For example, the measurement of the Higgs decay to WW^* in the WW fusion process determines

$$\sigma(H\nu_e\bar{\nu}_e) \times BR(H \rightarrow WW^*) \propto \frac{g_{HWW}^4}{\Gamma_H},$$

and thus the total width can be determined utilizing the model-independent measurement of g_{HWW} . In practice, a fit would be performed to all of the experimental measurements involving the Higgs boson couplings. [Table 6](#) lists the results of such a fit, applied using the expected statistical measurement precisions given in [Table 4](#) (scaled to include the benefits of electron polarization). Here it is assumed that CLIC operation above 1 TeV is primarily with -80% electron polarization to enhance the WW fusion cross section. These *preliminary fit results* do not yet include the constraints on the invisible width that can be obtained from the Higgs-strahlung process at $\sqrt{s} = 350$ GeV, and will be updated accordingly. The interpretation of the results listed in [Table 6](#) requires some care as the uncertainties on g_{HZZ} , g_{HWW} , g_{Hbb} , $g_{H\tau\tau}$, and $g_{H\tau\tau}$ are almost 100% correlated and are fixed by the precision to which g_{HZZ} can be determined; the uncertainties on the ratios of these couplings are typically *much smaller* than the uncertainties on the absolute values of the couplings.

Whilst the precise measurements of the Higgs couplings to gauge bosons, fermions and to itself are of interest in their own right, they will be crucial for testing the fundamental prediction of the Higgs mechanism that the Higgs coupling to different particles is proportional to their masses, as summarized in [Figure 8](#).

As an alternative to the model-independent approach discussed so far, a fit was performed using nine Higgs coupling scale factors defined as:

$$\kappa_i^2 = \frac{\Gamma_i}{\Gamma_i^{\text{SM}}},$$

where Γ_i and Γ_i^{SM} are the measurement and SM prediction for the partial width of an individual visible Higgs decay mode i . Here the total Higgs boson width is given by the sum of the nine considered partial decay widths. This is equivalent to the assumption of no invisible Higgs decays. In this scenario, the ratio of the fitted total Higgs width to its SM prediction can be calculated as:

$$\Gamma_{H,\text{model}} = \sum_i \kappa_i^2 \cdot BR_i^{\text{SM}}.$$

The SM expectations for the branching ratios assuming a Higgs mass of 126 GeV, BR_i^{SM} , were taken from [\[15\]](#). Theoretical uncertainties on the SM predictions were neglected in the fit. [Table 7](#) shows the obtained *preliminary* precisions on the Higgs coupling scale factors.

Table 6: The precision Higgs observables at CLIC after (i) an integrated luminosity of 500 fb^{-1} at $\sqrt{s} = 350 \text{ GeV}$, (ii) after an additional 1.5 ab^{-1} at $\sqrt{s} = 1.4 \text{ TeV}$, and (iii) after a further 2.0 ab^{-1} at $\sqrt{s} = 3.0 \text{ TeV}$. The results were obtained from the statistical measurement precisions quoted in Table 4, scaled up assuming that operation above 1 TeV is primarily with -80% electron beam polarization. The uncertainties are statistical only. The entries marked ‘tbd’ indicate that results for $\sqrt{s} = 3 \text{ TeV}$ have yet to be determined.

Parameter	Measurement precision		
	350 GeV 500 fb^{-1}	+1.4 TeV $+1.5 \text{ ab}^{-1}$	+3.0 TeV $+2.0 \text{ ab}^{-1}$
m_H	120 MeV	30 MeV	20 MeV
Γ_H	9.2%	8.5%	8.4%
λ	—	21%	10%
g_{HZZ}	2.1%	2.1%	2.1%
g_{HWW}	2.6%	2.1%	2.1%
g_{Hbb}	2.7%	2.1%	2.1%
g_{Hcc}	3.8%	2.3%	2.2%
$g_{H\tau\tau}$	4.0%	2.5%	tbd
$g_{H\mu\mu}$	—	10.7%	5.6%
g_{Htt}	—	4.5%	tbd

Table 7: The Higgs coupling scale factors at CLIC after (i) an integrated luminosity of 500 fb^{-1} at $\sqrt{s} = 350 \text{ GeV}$, (ii) after an additional 1.5 ab^{-1} at $\sqrt{s} = 1.4 \text{ TeV}$, and (iii) after a further 2.0 ab^{-1} at $\sqrt{s} = 3.0 \text{ TeV}$. The assumptions used for the determination of these parameters are explained in the text. All results were obtained from the statistical measurement precisions quoted in Table 4, scaled up assuming that operation above 1 TeV is primarily with -80% electron beam polarization. The uncertainties are statistical only. The entries marked ‘tbd’ indicate that results for $\sqrt{s} = 3 \text{ TeV}$ have yet to be determined.

Parameter	Measurement precision		
	350 GeV 500 fb^{-1}	+1.4 TeV $+1.5 \text{ ab}^{-1}$	+3.0 TeV $+2.0 \text{ ab}^{-1}$
$\Gamma_{H,\text{model}}$	1.6%	0.29%	0.22%
κ_{HZZ}	0.49%	0.33%	0.24%
κ_{HWW}	1.5%	0.15%	0.11%
κ_{Hbb}	1.7%	0.32%	0.19%
κ_{Hcc}	3.1%	1.1%	0.75%
$\kappa_{H\tau\tau}$	3.5%	1.4%	tbd
$\kappa_{H\mu\mu}$	—	10.5%	5.2%
κ_{Htt}	—	4.0%	tbd
κ_{Hgg}	3.6%	0.79%	0.56%
$\kappa_{H\gamma\gamma}$	—	5.5%	tbd

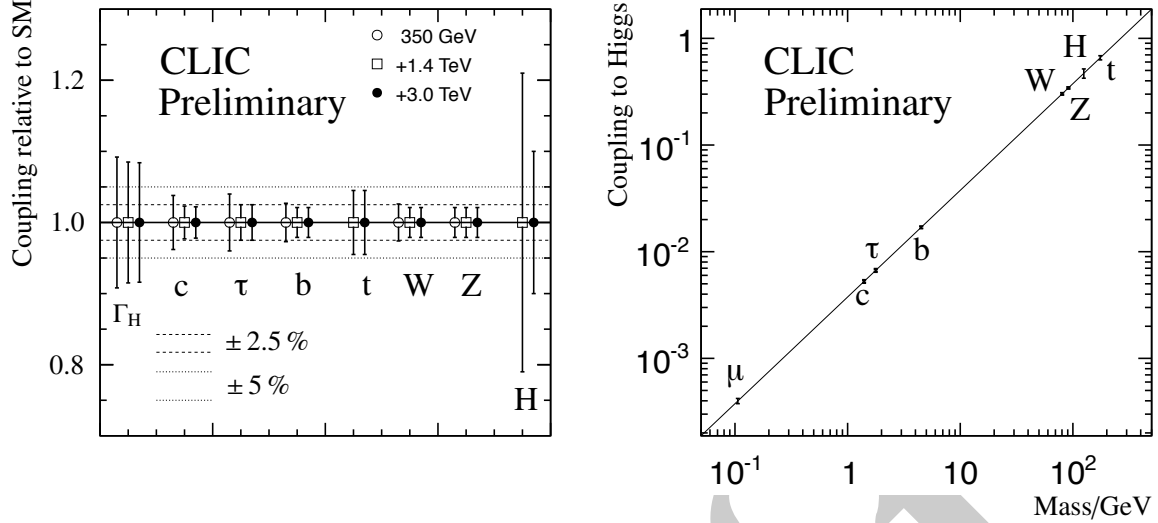


Fig. 8: An illustration of the typical precisions to which the relation between the Higgs couplings to the masses of the particles can be tested at CLIC. The left plot shows the precision achievable at CLIC after (i) an integrated luminosity of 500 fb^{-1} at $\sqrt{s} = 350 \text{ GeV}$, (ii) after an additional 1.5 ab^{-1} at $\sqrt{s} = 1.4 \text{ TeV}$, and (iii) after a further 2.0 ab^{-1} at $\sqrt{s} = 3.0 \text{ TeV}$. The listed values assume SM couplings. The right plot summarizes the precision of the test of the prediction of the proportionality of the Higgs coupling to mass (after the three assumed stages of CLIC operation). The sensitivities assume that operation above 1 TeV is primarily with -80% beam polarization.

2.5 Impact of the Precision Measurements of the Higgs Couplings

The precise measurements of the Higgs boson properties at CLIC would provide a powerful probe of the structure of the Higgs sector. The SM with a single Higgs doublet is only one of the possibilities. The model-independent measurements at CLIC would be crucial to distinguish between the different possible manifestations of the underlying physics. In many extended Higgs theories the lightest Higgs scalar can have nearly identical properties to the SM Higgs boson. In this decoupling limit, additional states of the Higgs sector are heavy and it may be difficult to detect them at the LHC. CLIC would provide sensitivity to new Higgs bosons beyond that achievable at the LHC, with states of masses up to essentially half the e^+e^- center-of-mass energy (see [Section 4.2](#)) being directly detectable. Nevertheless, if these massive states were very heavy, and therefore beyond the reach of the LHC and even CLIC, precision measurements would be crucial in order to distinguish the simple Higgs sector of the SM from a more complicated scalar sector.

Deviations from the SM can arise from an extended structure of the Higgs sector, for instance if there is more than one Higgs doublet. Another source of possible deviations from the SM Higgs properties are loop effects from BSM particles. The potential for probing the physics of EWSB is directly related to the sensitivity for verifying deviations from the SM. For example, in [Figure 9](#) the typical deviations from the SM predictions for a Two-Higgs-Doublet model are compared to the precision on the couplings achievable at the different energy stages of CLIC. In this example, the high-precision measurements at CLIC would clearly indicate the non-SM nature of the EWSB sector. To observe such deviations at the $> 3\sigma$ level, operation of CLIC at the higher energies is crucial.

Furthermore, small deviations from SM-like behavior can arise as a consequence of fundamentally different physics of EWSB. For example, if an additional fundamental scalar such as the radion mixes with the Higgs boson, the possibly small shifts in the branching ratios and overall decay width relative to the SM Higgs boson may only be discernible through the high-precision and model-independent measurements of couplings available at a future linear collider.

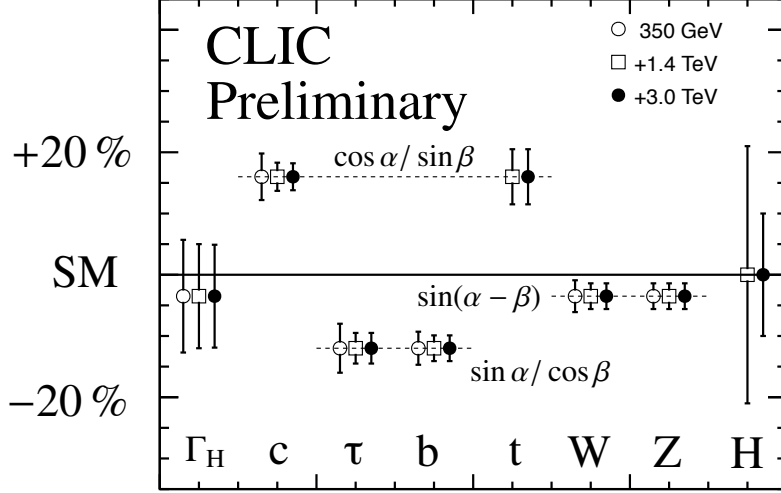


Fig. 9: Left: Typical deviations of the Higgs couplings to different particles from the SM predictions in a Two-Higgs-Doublet model. The CLIC precisions after the various energy stages are the same as in Figure 8.

2.6 Higgs Boson Mass, Spin and CP Properties

Detailed studies of the properties of the Higgs boson are possible at a high-luminosity e^+e^- linear collider. For example the Higgs boson mass can be determined to better than 100 MeV at CLIC operating at $\sqrt{s} = 350$ GeV from either the Z recoil mass distribution or from the direct reconstruction of the decay products. At higher center-of-mass energies the large samples of $H \rightarrow b\bar{b}$ decays would allow the Higgs mass to be determined with a statistical precision of about ± 30 MeV. At this stage the potential size of systematic uncertainties, such as the b-quark jet-energy scale, have not been assessed yet, although potential systematic biases could be mitigated using $Z \rightarrow b\bar{b}$ decays.

CLIC also provides the possibility of detecting CP violation in the Higgs sector, where *a priori* the observed Higgs state with $m_H = 125$ GeV can be an admixture of CP even and CP odd states. The most general model-independent expression for the HVV coupling can be written as

$$g_{HVV} = -gM_V \left[\alpha g_{\mu\nu} + \beta \left(\frac{(p \cdot q) g_{\mu\nu}}{M_V^2} - p_\nu q_\mu \right) + i\gamma \frac{\epsilon_{\mu\nu\rho\sigma} p^\rho q^\sigma}{M_V^2} \right],$$

where V represents either a W or Z boson, p and q are the four momenta of the two vector bosons, and $\epsilon_{\mu\nu\rho\sigma}$ is the totally antisymmetric tensor. For the SM Higgs boson, $\alpha = 1$ and $\beta = \gamma = 0$. In contrast, for a pure CP odd Higgs boson, $\alpha = \beta = 0$, and γ is expected to be small. Dedicated studies of the CP properties of the light Higgs boson have not yet been performed in the context of the CLIC study. Nevertheless, such studies have been performed for a e^+e^- linear collider operating at $\sqrt{s} = 350$ GeV. For example, by utilizing the angular correlations in $e^+e^- \rightarrow HZ \rightarrow 4f$ it was demonstrated that η , which parameterizes the mixing between a CP-even and a CP-odd Higgs state, could be measured with an accuracy of 3% – 4% [16]. As part of the future CLIC study, it is intended to extend these studies to CLIC operating above 1 TeV.

3 Top Physics

3.1 Introduction

As the heaviest elementary particle known to date, the top quark is of particular interest. It couples most strongly to the Higgs field, and due to its high mass also provides leading contributions in higher order corrections to many processes and may provide high sensitivity to physics beyond the SM. Together with the Higgs mass, the top mass is a key input to studies of the stability of the SM vacuum, which can be seen as an upper validity bound of the SM. With the precision of the Higgs mass provided by the LHC today, the uncertainty of the top mass is the leading uncertainty in this evaluation. Improvements in the measurement of the top quark mass, possible at a linear collider, will substantially reduce these uncertainties. At the same time, the precise measurement of couplings of the top quark to the Higgs and to gauge bosons will provide the possibilities for precision tests of SM predictions and a corresponding sensitivity to New Physics at higher scales.

3.2 Top Quark Mass Measurements at CLIC

An e^+e^- collider offers two complementary ways of measuring the top quark mass; by direct reconstruction of the invariant mass of the decay products, and through a scan of the top pair production threshold. While the former measurement can be performed at essentially arbitrary energies above threshold, the latter requires collider operations at several closely-spaced energies around the pair production threshold. The theoretical interpretation of the two measurements differ considerably. The invariant mass is interpreted by comparing the measured distribution with that predicted by MC simulations, and as such is obtained in the context of the used event generator and is thus not defined in a theoretically rigorous way. Progress has been made in the calculation of non-perturbative effects which affect the final state of $t\bar{t}$ decays, but uncertainties remain substantial. The cross section evolution around threshold is calculated to higher orders in theoretically well-defined mass schemes, providing a clean interpretation of the top quark mass obtained from a threshold scan.

The prospects for top mass measurements at CLIC using both techniques have been studied in full simulations, taking beam-induced and non- $t\bar{t}$ physics background as well as realistic luminosity spectra into account [17]. With $t\bar{t}$ cross sections of 450 fb at 350 GeV and 530 fb at 500 GeV, integrated luminosities of 100 fb^{-1} result in several ten thousand $t\bar{t}$ pairs, enabling measurements with high statistical precision. For both techniques, the two dominating decay modes of the $t\bar{t}$ pair are considered, the fully-hadronic decay $t\bar{t} \rightarrow W^+bW^-\bar{b} \rightarrow q\bar{q}bq\bar{q}\bar{b}$ and the semi-leptonic decay $t\bar{t} \rightarrow W^+bW^-\bar{b} \rightarrow q\bar{q}bl\nu\bar{b}$, where τ final states are rejected. Together, these decays account for a branching fraction of 75% and provide events that can be precisely identified and reconstructed. Top pair identification and reconstruction is performed by a combination of flavor tagging, kinematic fitting and multivariate background rejection, resulting in highly pure signal samples. **Figure 10** (left) shows the reconstructed invariant mass of fully-hadronic top pair decays, together with the remaining non- $t\bar{t}$ background for an integrated luminosity of 100 fb^{-1} at an energy of 500 GeV. The mass is determined with a maximum likelihood fit also shown in the figure. **Figure 10** (right) illustrates a ten-point scan of the $t\bar{t}$ production threshold corresponding to a total integrated luminosity of 100 fb^{-1} . The sensitivity to the 1S top mass is illustrated by showing the variations of the threshold behavior for different masses. The top quark mass and the strong coupling constant are extracted simultaneously from a two-dimensional template fit of the measured cross section. **Table 8** summarizes the achieved statistical precision. In addition to these statistical uncertainties, possible systematic uncertainties have been evaluated. For the invariant mass it was found that jet energy scale systematics can be constrained to a level comparable to the statistical uncertainty. However, since the measurement itself is performed in the context of a leading order event generator, the interpretation of the result in theoretically well-defined mass schemes results in substantial additional uncertainties, expected to be larger than the purely experimental uncertainties quoted here. For the threshold scan, a

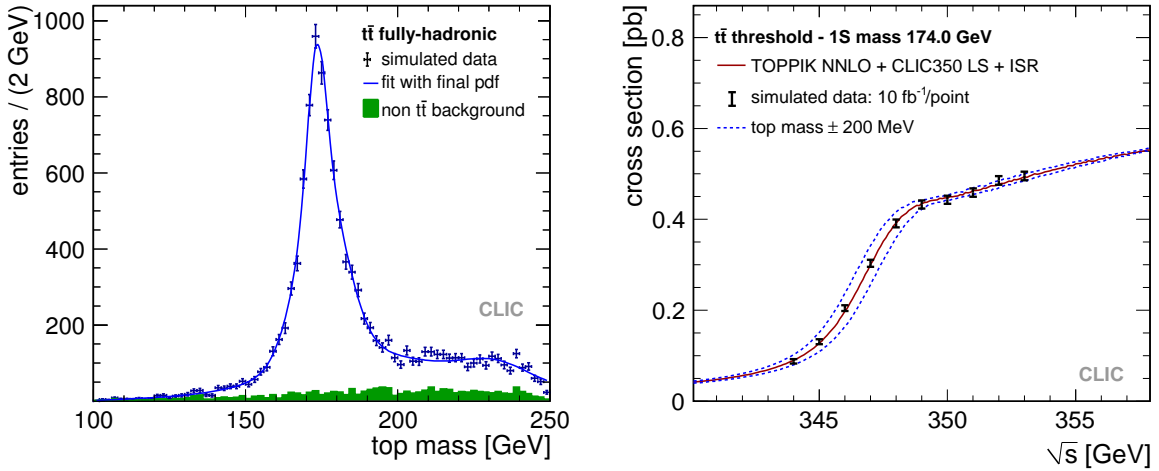


Fig. 10: Left: Reconstructed top quark mass in the all-hadronic decay channel for an integrated luminosity of 100 fb^{-1} at 500 GeV. The top mass and width is determined with an unbinned maximum likelihood fit to the invariant mass distribution, shown by the solid line. Right: Illustration of a scan of the top quark pair production threshold, with each point corresponding to 10 fb^{-1} of integrated luminosity. The sensitivity to the top quark mass is illustrated by showing the cross section also for 200 MeV changes in mass.

Table 8: Summary of full detector simulation results obtained under realistic CLIC beam conditions in the top quark studies.

\sqrt{s} (GeV)	Technique	Measured quantity	Integrated luminosity (fb^{-1})	Unit	Generator value	Stat. error
350	Threshold scan	Mass	10×10	GeV	174	0.033
		α_s			0.118	0.0009
500	Invariant mass	Mass	100	GeV	174	0.080

statistical uncertainty of the top quark mass in the 1S scheme of 33 MeV is obtained, resulting in a total uncertainty of approximately 100 MeV when including theoretical normalisation uncertainties as well as analysis-related and beam energy systematics. Additional theory uncertainties on the order of 100 MeV enter when transforming the 1S mass used in the threshold scan analysis to the $\overline{\text{MS}}$ mass scheme commonly used in electroweak precision calculations. Given the dominance of systematic uncertainties in the mass determination via a threshold scan, the difference between different e^+e^- collider options is not expected to impact visibly on the total uncertainty [17].

3.3 Top as a Probe for New Physics

The high mass of the top quark and its correspondingly strong coupling to the mechanism of electroweak symmetry breaking make it a promising probe for New Physics. For example, the measurement of forward-backward and left-right asymmetries, where the latter makes use of polarized beams provided by a linear collider, provides a high sensitivity to extra-dimensional models and new heavy gauge bosons by probing the $t\bar{t}Z$ and $t\bar{t}\gamma$ vertices with high precision. The fact that the top quark decays before it hadronizes, allowing access to its polarization by the analysis of angular distributions of the decay products, makes it a sensitive probe for the couplings to gauge bosons and provides the possibility to search for CP violation in the top sector.

So far, no full simulation studies on these topics have been carried out in the context of CLIC, but the sensitivity of asymmetry measurements to different New Physics models has been studied extensively for the ILC [18]. These studies achieve a 1% precision on the couplings, providing sensitivity for example to Kaluza–Klein particles up to masses of tens of TeV. The higher energy at CLIC will allow one to eliminate uncertainties in the assignment of b jets to W bosons due to the higher boost of the quarks and the corresponding better separation of the decay products of the t and \bar{t} , one of dominating experimental challenges at the ILC at 500 GeV. This may result in an increased physics reach, but still requires dedicated studies. Another benefit of the high center-of-mass energy of CLIC is that in most approaches to New Physics affecting the top quark observables, the relative contribution from New Physics increases with the interaction energy E as E^2/Λ^2 , where Λ represents the scale of New Physics. Examples for this are the Kaluza–Klein excitation scale, the mass of an extra gauge boson, or the suppression scale of a higher-dimensional operator contributing to $t\bar{t}$ production.

The high granularity of the detectors together with the particle flow event reconstruction enables the clean reconstruction also of highly boosted top quarks, with a measurement of the individual decay products from an analysis of the jet substructure. The availability of these techniques forms the basis for precision physics with top quarks in the multi-TeV regime. Topics to be investigated in detail in the future include the study of top production asymmetries, the couplings to γ , Z, W and H bosons, the sensitivity to CP violation in the top sector and flavor changing top decays.

3.4 Conclusion

Top physics is an integral part of the CLIC physics program. The first stage will provide a precise measurement of the top quark mass on the 100 MeV level and measurements of other top properties such as the width, while higher energy stages give access to various measurements sensitive to New Physics. The achievable precision for the mass measurements has already been investigated in detail in full simulations, including incomplete studies of systematic uncertainties. The potential to use top quarks as a probe for New Physics will be the subject of studies in the near future, which will include:

- top quark production asymmetries;
- top couplings to γ , Z, W and H bosons;
- CP violation in the top sector;
- flavor changing top decays.

4 BSM Searches

4.1 Introduction

It is generally acknowledged that the Standard Model is not the complete picture of particle physics. The quest for a deeper understanding of dark matter, baryon asymmetry of the universe, CP violation, the flavor problem, unification, and stability of the Higgs sector gives rise to a wide spectrum of ideas that extend our theories beyond what the Standard Model can provide.

In this section we give a few examples of how a high-energy e^+e^- CLIC machine can discover and study physics beyond the Standard Model. In [Section 4.2](#) we discuss the discovery potential and study prospects for supersymmetry, which remains a leading idea of physics beyond the Standard Model. In [Section 4.3](#) we consider the possibility of a composite Higgs boson, and compare the search sensitivities for its composite nature at CLIC versus LHC. In [Section 4.4](#) we briefly discuss how additional exotic physics cases can be discerned through careful measurements of high-energy final states. Our primary example is that of a Z' boson.

4.2 Supersymmetry

Supersymmetry was posited many years ago as a natural extension of the spacetime structure bearing a symmetry between bosons and fermions. Over time it was recognized that there are many other features that speak for its existence, including having a natural dark matter candidate, revealing a possible unification of the forces at high energies, and having the ability to solve the electroweak scale hierarchy problem. This latter consideration has been under some strain given that the LHC has not yet found superpartners, and it has found a Higgs boson mass of 125 GeV, which may appear to be unnaturally heavy for the minimal model. Nevertheless, these two facts are mutually compatible and higher energy LHC runs are needed to cover more ground in the supersymmetry parameter space.

If supersymmetry is found it will be of primary importance to study all the masses and couplings to high precision to test the many ideas of how supersymmetry can be composed. CLIC offers this opportunity. [Table 9](#) shows the excellent precision by which one can measure the superpartner mass spectrum at CLIC. The table includes results from the example models *I*, *II*, and *III* which are detailed in the CDR [[5](#), [6](#), [19](#), [20](#)]. Accessible states are measured to better than a few percent uncertainty with standard assumptions on the energy and luminosity of CLIC. See the table caption for more details.

CLIC allows one to perform precise measurements of the superpartners even using fully hadronic final states which are very difficult at hadron colliders. [Figure 11](#) shows an example for a final state with four jets and missing energy. This figure also demonstrates the suppression of pileup from beam-induced backgrounds as introduced in [Section 1](#). The mass and pair production cross section for the lightest chargino were extracted from the reconstructed W energy distribution in $e^+e^- \rightarrow \tilde{\chi}^+\tilde{\chi}^- \rightarrow q\bar{q}q\bar{q}W^+W^-$ events at 1.4 TeV. Statistical precisions of 0.2% for the mass of 487 GeV and 1.3% for the pair production cross section of 15.3 fb were obtained assuming an integrated luminosity of 1.5 ab^{-1} .

Supersymmetry is necessarily (at least) a Two-Higgs-Doublet theory, and a full demonstration of the theory and a full test of its underlying structure requires measuring the four heavier Higgs degrees of freedom, H^\pm , A and H . [Figure 12](#) shows the ability to measure these masses to the percent level, and to distinguish the mass splitting among all of these states, which can be crucial for understanding the underlying model.

It should be noted also that two Higgs doublet theories are not necessarily restricted to supersymmetry, therefore this study has a much broader implication than just supersymmetric Higgs boson searches. Indeed, in a broader sense all of these searches have wider applicability than only supersymmetry, since the particles under consideration can be classified simply as states with given mass, spin and quantum numbers, which can show up in any theory, supersymmetric or not.

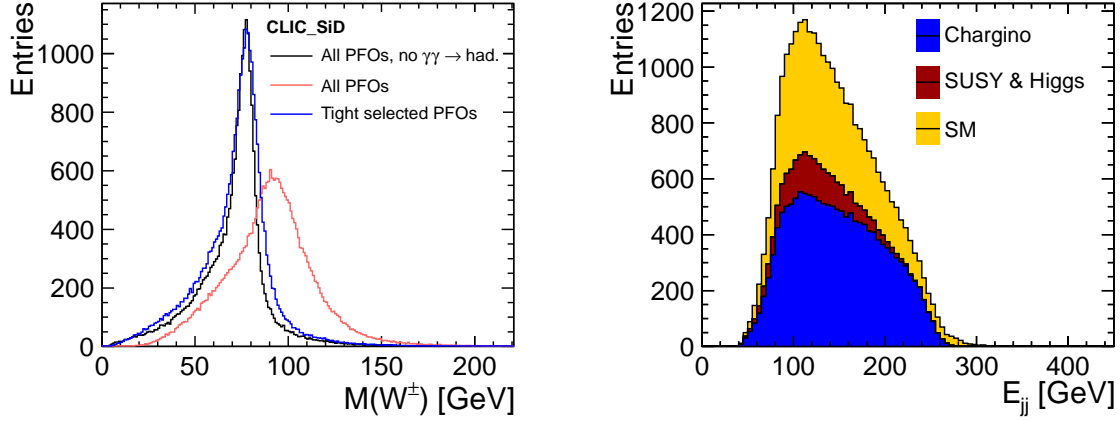


Fig. 11: Left: Reconstructed mass of W^\pm candidates in $e^+e^- \rightarrow \tilde{\chi}_1^+ \tilde{\chi}_1^- \rightarrow q\bar{q}q\bar{q}W^+W^-$ events at 1.4 TeV without overlay of $\gamma\gamma \rightarrow \text{hadrons}$ (black histogram), with overlay of $\gamma\gamma \rightarrow \text{hadrons}$ (red histogram) and using selected reconstructed particles (blue histogram). Right: Di-jet invariant mass distribution for the selected signal and background events in the same channel. A full simulation of the CLIC_SiD detector is used. All distributions are scaled to an integrated luminosity of 1.5 ab^{-1} .

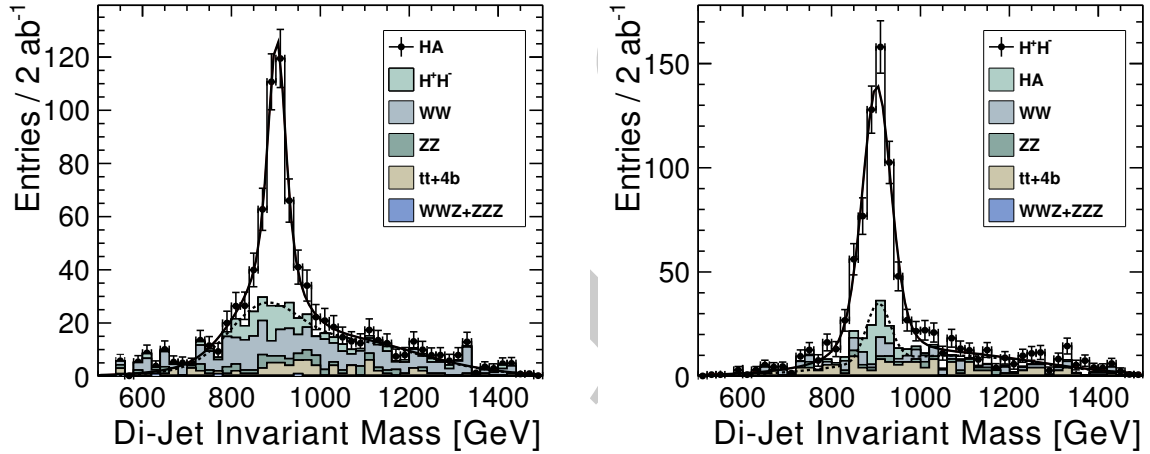


Fig. 12: Di-jet invariant mass distributions for the $b\bar{b}b\bar{b}$ (left) and $t\bar{b}b\bar{t}$ (right) final states at 3 TeV for *model I*. The distributions for the $e^+e^- \rightarrow HA$ and $e^+e^- \rightarrow H^+H^-$ processes and for the individual backgrounds are shown separately. A full simulation of the CLIC_ILD detector is used. All distributions are scaled to an integrated luminosity of 2 ab^{-1} .

4.3 Composite Higgs Boson Theories

Since a fundamental scalar boson has quadratic sensitivities to higher scales it is susceptible to quadratically divergent corrections that can destabilize its potential and small mass. Supersymmetry solves this problem via a symmetry, but there are other ways to attempt to solve the problem. A favored option that is not excluded by current LHC data is that the Higgs boson is not a fundamental scalar, but rather a composite state of fermions. In this way electroweak symmetry breaking and mass generation are at their essence a condensation of multiple fields together, whose composite nature mimics a condensing scalar boson – the Higgs boson.

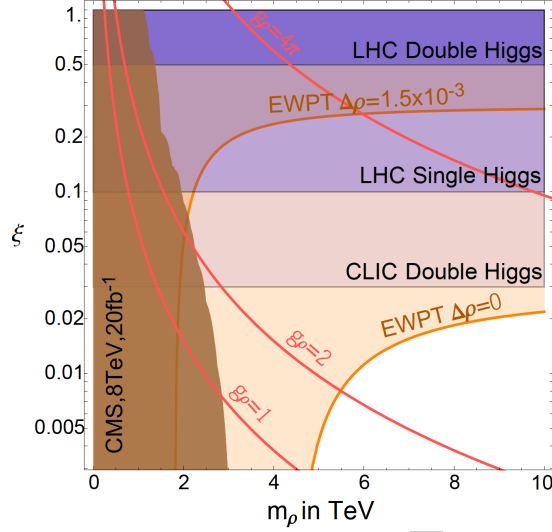


Fig. 13: Summary plot of the current constraints and prospects for direct and indirect probes of the strong interactions triggering electroweak symmetry breaking. m_ρ is the mass of the vector resonances and $\xi = (v/f)^2$ measures the strengths of the Higgs interactions. The dark brown region on the left shows the current combined limit from direct production of the charged ρ^\pm at the LHC decaying to $\ell\nu$ and $WZ \rightarrow 3\ell\nu$ final states. The dark (medium light) horizontal purple bands indicate the sensitivity on ξ expected at the LHC from double (single) Higgs production with 300 fb^{-1} of integrated luminosity. The pink horizontal band reports the sensitivity reach on ξ from the study of double Higgs processes alone at CLIC with 1 ab^{-1} of integrated luminosity at 3 TeV. Finally, experimental electroweak precision tests (EWPT) favor the region below the orange thick line with and without additional contribution to ϵ_1 . The Higgs mass is assumed to be 125 GeV and the vector resonance contribution to ϵ_3 is taken to be $\Delta\epsilon_3 = m_W^2/m_\rho^2$. The domain of validity of our predictions, $g_\rho < 4\pi$, is below the upper red line (From [21]).

The phenomenology of composite Higgs theories is very similar to the phenomenology of the SM Higgs boson. The only difference is that every observable has relative corrections to it that are proportional to $\xi = (v/f)^2$, where $v \simeq 246 \text{ GeV}$ is the normal vacuum expectation value of the “Higgs”, and f is the (higher) scale of compositeness. The scale f cannot be too small otherwise corrections to normal Higgs production and decay are $\xi = \mathcal{O}(1)$ which is forbidden by current data. Therefore, $\xi \ll 1$ is required. Exactly how low needs to be derived carefully from data.

Figure 13 (from [5]) shows the sensitivities at LHC and CLIC for observing non-SM signatures from the composite nature of the Higgs boson in the plane of ξ and m_ρ , where ρ is the vector resonance of the composite theory, in direct analogy to the ρ of QCD which regularizes composite pion phenomenology. A detailed description of Figure 13 is given in the caption. With an integrated luminosity of 1 ab^{-1} accumulated at 3 TeV, CLIC can reach $\xi \approx 0.03$ independent of m_ρ due to the relatively clean environment for studying double Higgs boson production. The reach on ξ can be improved significantly when combining precision results from the combined CLIC Higgs coupling fit with double Higgs production and was estimated to be around $\xi = 0.002$ [21], corresponding to a Higgs composite scale of 70 TeV. For comparison, the LHC with an integrated luminosity of 300 fb^{-1} at 14 TeV can reach only down to $\xi \approx 0.1$, given the most recent estimates.

4.4 Search for Exotic Physics through Direct Production and Precision Studies

CLIC is a precision e^+e^- machine, and as such it is able to study many different observables with sub-percent accuracy. For example $e^+e^- \rightarrow f\bar{f}$ observables can be key to seeing small deviations with respect

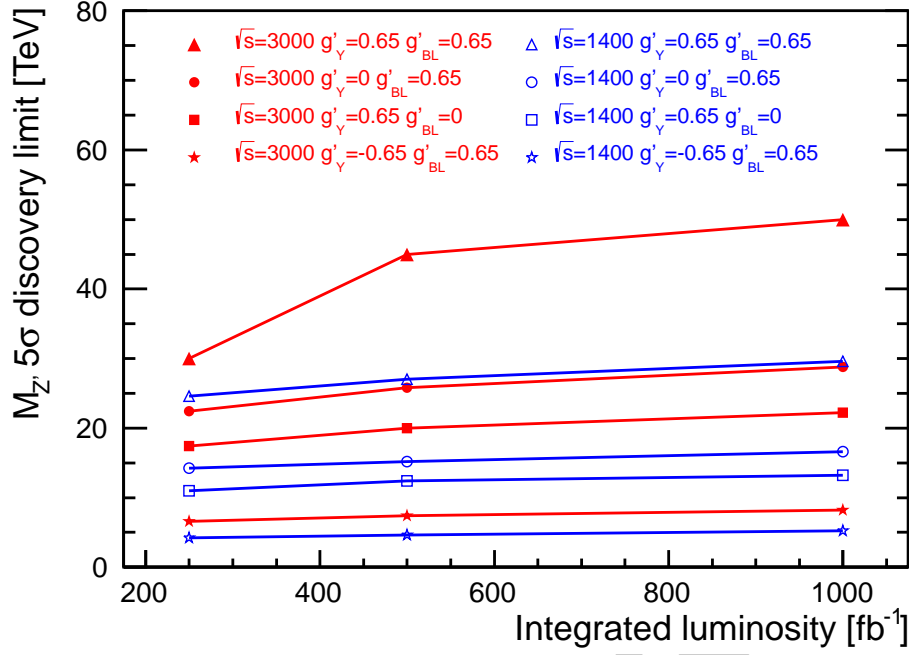


Fig. 14: 5σ limit for a $M_{Z'}$ discovery as function of the integrated luminosity for different values of the couplings g_Y' and g_{BL}' . The limits shown are determined from the combined observables σ and A_{FB} at $\sqrt{s} = 3$ TeV and 1.4 TeV.

to the SM when lepton scattering energies are in the TeV region. The observables include total cross section, forward-backward asymmetry, and polarization asymmetries. In general one can put strong constraints on higher-dimensional operators that connect electrons to muons, for example, from these precision studies of $e^+e^- \rightarrow \mu^+\mu^-$. A concrete case of this impressive general capacity is sensitivity to a new Z' that couples to leptons [22]. The new Z' is the most general $U(1)'$ gauge symmetry that is anomaly-free with respect to the SM particle content. Under this $U(1)'$ the SM fermions have charge $g_Y'(Y_f) + g_{BL}'(B - L)_f$. Figure 14 shows 5σ discovery limits for Z' gauge boson mass as a function of the achieved integrated luminosity of the machine using the measured cross section and asymmetries. It was found, for example, that there are regions of parameter space for this anomaly free Z' theory where sensitivity of the mass reaches into several tens of TeV, well beyond the center-of-mass energy of the machine, and well beyond what the LHC or its conceived upgrades can achieve. This impressive result is characteristic of many such studies that can be mapped to a non-renormalizable operator that connects the electrons to any “clean” final state, such as muons or gauge bosons.

4.5 Conclusion

In our discussion of some of the leading ideas of physics beyond the SM we have found significant discovery potential. In addition, Table 10 gives a brief survey of discovery reach of the CLIC collider compared to the LHC and its possible high-luminosity upgrades in various other beyond the SM theories. It is adapted from the CLIC CDR [5]. As illustrated in our examples earlier in the text and in Table 10, some indirect precision studies allow the discovery of signals beyond the SM originating from scales well beyond the center-of-mass energy of the collider. We have also seen that if particles are discovered at CLIC or the LHC, CLIC has the ability to measure the masses and couplings at the percent level or better. This is generally far more precise than what a hadron collider can do alone. The precision studies complementary to the LHC and the stand-alone discovery and precision capacity of CLIC makes it an ideal machine for extending our search for physics beyond the SM. Future effort in beyond the SM physics will include

- Searches for dark matter missing energy signatures in a model-independent way;
- Searches and study of resonances associated with composite Higgs theory;
- Generalization of higher-dimensional effective operator searches at the various stages of CLIC running;
- Searches for very weakly interacting exotic particles;
- Searches for vectorlike particles charged under electroweak group;
- Responding to theory guidance for New Physics that is compatible and explains LHC data in the future.

Table 9: Summary table of the CLIC SUSY benchmark analyses results obtained with full-detector simulations with background overlaid. All studies are performed at a center-of-mass energy of 3 TeV (1.4 TeV) and for an integrated luminosity of 2 ab⁻¹ (1.5 ab⁻¹) [23, 24, 25, 26, 27, 28, 29].

\sqrt{s} (TeV)	Process	Decay mode	SUSY model	Measured quantity	Generator value (GeV)	Stat. uncertainty
3.0	Sleptons	$\tilde{\mu}_R^+ \tilde{\mu}_R^- \rightarrow \mu^+ \mu^- \tilde{\chi}_1^0 \tilde{\chi}_1^0$	II	$\tilde{\ell}$ mass	1010.8	0.6%
				$\tilde{\chi}_1^0$ mass	340.3	1.9%
		$\tilde{e}_R^+ \tilde{e}_R^- \rightarrow e^+ e^- \tilde{\chi}_1^0 \tilde{\chi}_1^0$		$\tilde{\ell}$ mass	1010.8	0.3%
				$\tilde{\chi}_1^0$ mass	340.3	1.0%
		$\tilde{\nu}_e \tilde{\nu}_e \rightarrow \tilde{\chi}_1^0 \tilde{\chi}_1^0 e^+ e^- W^+ W^-$		$\tilde{\ell}$ mass	1097.2	0.4%
				$\tilde{\chi}_1^\pm$ mass	643.2	0.6%
3.0	Chargino Neutralino	$\tilde{\chi}_1^+ \tilde{\chi}_1^- \rightarrow \tilde{\chi}_1^0 \tilde{\chi}_1^0 W^+ W^-$	II	$\tilde{\chi}_1^\pm$ mass	643.2	1.1%
		$\tilde{\chi}_2^0 \tilde{\chi}_2^0 \rightarrow h/Z^0 h/Z^0 \tilde{\chi}_1^0 \tilde{\chi}_1^0$		$\tilde{\chi}_2^0$ mass	643.1	1.5%
3.0	Squarks	$\tilde{q}_R \tilde{q}_R \rightarrow q \bar{q} \tilde{\chi}_1^0 \tilde{\chi}_1^0$	I	\tilde{q}_R mass	1123.7	0.52%
3.0	Heavy Higgs	$H^0 A^0 \rightarrow b \bar{b} b \bar{b}$	I	H^0/A^0 mass	902.4/902.6	0.3%
		$H^\pm H^\mp \rightarrow t \bar{b} b \bar{t}$		H^\pm mass	906.3	0.3%
1.4	Sleptons	$\tilde{\mu}_R^+ \tilde{\mu}_R^- \rightarrow \mu^+ \mu^- \tilde{\chi}_1^0 \tilde{\chi}_1^0$	III	$\tilde{\ell}$ mass	560.8	0.1%
				$\tilde{\chi}_1^0$ mass	357.8	0.1%
		$\tilde{e}_R^+ \tilde{e}_R^- \rightarrow e^+ e^- \tilde{\chi}_1^0 \tilde{\chi}_1^0$		$\tilde{\ell}$ mass	558.1	0.1%
				$\tilde{\chi}_1^0$ mass	357.1	0.1%
		$\tilde{\nu}_e \tilde{\nu}_e \rightarrow \tilde{\chi}_1^0 \tilde{\chi}_1^0 e^+ e^- W^+ W^-$		$\tilde{\ell}$ mass	644.3	2.5%
				$\tilde{\chi}_1^\pm$ mass	487.6	2.7%
1.4	Stau	$\tilde{\tau}_1^+ \tilde{\tau}_1^- \rightarrow \tau^+ \tau^- \tilde{\chi}_1^0 \tilde{\chi}_1^0$	III	$\tilde{\tau}_1$ mass	517	2.0%
1.4	Chargino Neutralino	$\tilde{\chi}_1^+ \tilde{\chi}_1^- \rightarrow \tilde{\chi}_1^0 \tilde{\chi}_1^0 W^+ W^-$	III	$\tilde{\chi}_1^\pm$ mass	487	0.2%
		$\tilde{\chi}_2^0 \tilde{\chi}_2^0 \rightarrow h/Z^0 h/Z^0 \tilde{\chi}_1^0 \tilde{\chi}_1^0$		$\tilde{\chi}_2^0$ mass	487	0.1%

Table 10: Discovery reach of various theory models for different colliders [5]. LHC at $\sqrt{s} = 14$ TeV assumes 100 fb^{-1} of integrated luminosity, while HL-LHC is with 1 ab^{-1} , and CLIC3 is $\sqrt{s} = 3$ TeV with up to 2 ab^{-1} . TGC is short for Triple Gauge Coupling, and “ μ contact scale” is short for LL μ contact interaction scale Λ with $g = 1$.

New particle	LHC (14 TeV)	HL-LHC	CLIC3
squarks [TeV]	2.5	3	$\lesssim 1.5$
sleptons [TeV]	0.3	-	$\lesssim 1.5$
Z' (SM couplings) [TeV]	5	7	20
2 extra dims M_D [TeV]	9	12	20–30
TGC (95%) (λ_γ coupling)	0.001	0.0006	0.0001
μ contact scale [TeV]	15	-	60
Higgs composite scale [TeV]	5–7	9–12	70

5 Precision Study of Electroweak Interactions

One of the tasks of an e^+e^- collider is to test the Standard Model electroweak predictions with high precision. In [Section 2](#) we have detailed the expectations of precision measurements for the Higgs boson sector, which is the most pressing electroweak precision program of the linear collider.

Likewise, we have seen that the precision measurement capabilities of CLIC in the presence of New Physics are well supported by recent analyses briefly described earlier in [Section 4](#). In the example case of supersymmetry, we see that superpartner masses can be measured to sub-percent accuracy. The masses of exotic heavy Higgs bosons also can be measured to this precision, as demonstrated in [Section 4](#). This excellent precision will reflect itself in whatever New Physics may be found in the high-energy frontier.

Another aspect of the precision electroweak program is to measure Standard Model processes to unprecedented levels to test self-consistency of the Standard Model framework. The observables most often considered in this context are the mass of the W boson, the weak mixing angle $\sin^2 \theta_W$ measured at various energies for various final state particles, and anomalous triple and quartic gauge boson couplings. There have been few CLIC studies up to this point on these pure electroweak precision processes in the context of the CLIC collider. However, as is the case with other measurements, we expect the results for lower-energy stages of CLIC to be comparable to the results found for the ILC, and we expect that some improvement can arise at the higher-energy and higher-luminosity phases of CLIC.

Large numbers of W bosons will be produced in $ee \rightarrow eW\nu$ events at a high-energy CLIC collider. Including the effects from ISR and Beamstrahlung, 22×10^6 events for 1.5 ab^{-1} of data collected at 1.4 TeV and 45×10^6 events for 2 ab^{-1} of data collected at 3 TeV are expected assuming unpolarized beams. It was found in a generator-level study that the number of hadronic W decays expected is 9×10^6 at 1.4 TeV and 15×10^6 at 3 TeV. Both jets from the W decay were requested to be the central region, i.e. $|\cos(\theta^{\text{jet}})| < 0.94$. These samples provide the potential for a competitive measurement of the W boson mass using its hadronic decays. A full simulation study is foreseen to study the impact of systematic effects like uncertainty of the jet energy scale on this measurement.

Regarding the anomalous triple gauge boson vertices, the CP-even couplings are defined in [\[30, 31\]](#) to arise from operators in the Lagrangian

$$\Delta\mathcal{L} = ig_1^V(W_{\mu\nu}^\dagger W^\mu V^\nu - W_\mu^\dagger V_\nu W^{\mu\nu}) + i\kappa_V W_\mu^\dagger W_\nu V^{\mu\nu} + \frac{i\lambda_V}{M_W^2} W_{\lambda\mu}^\dagger W_\nu^\mu V^{\nu\lambda} \quad (1)$$

$$-g_4^V W_\mu^\dagger W_\nu (\partial^\mu V^\nu + \partial^\nu V^\mu) + g_5^V \epsilon^{\mu\nu\rho\sigma} (W_\mu^\dagger \partial_\rho W_\nu + \partial_\rho W_\mu^\dagger W_\nu) V_\sigma \quad (2)$$

with the normalization $g_1^V = \kappa_V = 1$ and $\lambda_V = g_4^V = g_5^V = 0$ in the Standard Model at tree level. $\Delta g_1^V \equiv g_1^V - 1$ and $\Delta\kappa_V = \kappa_V - 1$ define shifts away from the Standard Model values.

The anomalous triple gauge couplings have been studied for CLIC in the past [\[32\]](#). These studies are not at the same mature full-simulation level that the more recent CLIC studies engage; however, they are expected to be reasonable estimates of what can be achieved in the high-energy CLIC environment. [Table 11](#) reproduces the results from [\[32\]](#) from precision $e^+e^- \rightarrow W^+W^-$ analysis, where the various couplings are defined in [\[30, 32\]](#). The superscripts L (R) refer to the values obtained for amplitudes with left (right) handed electrons and right (left) handed positrons. The definition for g_1 for example is from the combinations

$$g_1^L = 4\sin^2 \theta_W g_1^\gamma + (2 - 4\sin^2 \theta_W) g_1^Z \xi \quad (3)$$

$$g_2^R = 4\sin^2 \theta_W g_1^\gamma - 4\sin^2 \theta_W g_1^Z \xi \quad (4)$$

where $\xi = s/(s - m_Z^2)$. For more details, see [\[32\]](#).

The improvements in the sensitivity of these couplings can be derived from statistical arguments and analysis of the cross section scaling. One finds that for the couplings that derive from gauge-invariant

Table 11: Sensitivity of the real parts of CP-even couplings in units of 10^{-3} , defined and expounded upon in [32]. The integrated luminosities for the 500 GeV, 800 GeV and 3000 GeV stages are assumed here to be 500 fb^{-1} , 1 ab^{-1} and 3 ab^{-1} respectively.

\sqrt{s} [GeV]	$\text{Re}(\Delta g_1^L)$	$\text{Re}(\Delta \kappa_L)$	$\text{Re}(\lambda_L)$	$\text{Re}(g_5^L)$	$\text{Re}(g_1^R)$	$\text{Re}(\Delta \kappa_R)$	$\text{Re}(\lambda_R)$	$\text{Re}(g_5^R)$
500	2.6	0.85	0.59	2.0	10	2.4	3.6	6.7
800	1.6	0.35	0.24	1.4	6.2	0.92	1.8	4.8
3000	0.93	0.051	0.036	0.88	3.1	0.12	0.36	3.2

dimension-six operators with two derivatives, such as the λ_i couplings, the improvement in sensitivity to the anomalous couplings scales as $\sqrt{s \mathcal{L}_{\text{int}}}$, where s is the center-of-mass energy squared of the collision and \mathcal{L}_{int} is the integrated luminosity. The strength of this improvement derives from the fact that the higher dimension operator has derivatives that turn to energy factors in the numerator of the correction factor. Numerically, this implies that the value of 0.59 obtained for $\text{Re}(\lambda_L)$ at $\sqrt{s} = 500 \text{ GeV}$ becomes 0.26 for the 800 GeV stage and 0.04 for the 3000 GeV stage, which is close to the 0.24 and 0.036 actual values found in [32] and shown here in Table 11. The significant improvements of the sensitivity to these couplings with increased energy, as can be seen in this study, has been recognized for some time now [31].

There is not necessarily an equivalently simple statistical scaling argument for the g_i and $\Delta \kappa$ couplings, as their definition is to disrupt the gauge-invariant renormalizable couplings of the Standard Model. A calculation of the energy dependence of the cross section is needed for each stage in these cases. The energy scaling for $\Delta \kappa$ turns out to be similar to that of the λ_i couplings, and so significant improvement takes place. The anomalous g_i couplings do not have the same scaling; nevertheless, the analysis of [32] as shown in the table shows that modest improvements of their sensitivities occur with increased energy and luminosity.

The precision electroweak measurements program at CLIC will proceed in the future with full simulations of relevant observables. This activity includes

- Simulations of triple and quartic gauge boson vertex corrections to $e^+e^- \rightarrow W^+W^-(\nu\nu/e^+e^-)$;
- Simulations of the forward–backward and left–right asymmetries of fermion production to achieve precision measurements of $\sin^2 \theta_f^{\text{eff}}$ at various energy stages;
- Simulations of W boson mass determination at high energy and high luminosity;
- Simulations of total $e^+e^- \rightarrow f\bar{f}$ cross sections at high energy with various electron–positron polarizations in search of form-factor suppressions or enhancements.

6 Summary and Conclusions

The CLIC accelerator is an attractive option for a future high-energy e^+e^- linear collider operating at center-of-mass energies up to 3 TeV. The feasibility of the CLIC accelerator was demonstrated through extensive prototyping, simulations and large-scale tests, as described in the conceptual design report [4]. The physics reach of CLIC was studied in detail and the majority of the results described in this document are based on full detector simulation and event reconstruction, taking into account the pile-up of background from $\gamma\gamma \rightarrow \text{hadrons}$.

This report summarises the physics potential of CLIC operating in three distinct energy stages. The first stage at $\sqrt{s} \approx 350$ GeV provides precise measurements of the properties of the Higgs boson and the top quark. Subsequent high-energy running, here taken to be at $\sqrt{s} = 1.4$ TeV and $\sqrt{s} = 3.0$ TeV, provides the potential to accumulate large samples of Higgs boson decays providing a range of Higgs boson couplings at the $\mathcal{O}(2\%)$ level, going significantly beyond what is achievable at the HL-LHC. This level of precision may be necessary to distinguish the light Higgs boson of an extended theory from a Standard Model Higgs boson. Furthermore, high-energy CLIC operation allows to measure the Higgs trilinear self-coupling parameter λ at the 10% level. In addition to probing the electroweak symmetry breaking mechanism, the operation of CLIC at $\sqrt{s} > 1$ TeV would provide sensitivity to a wide range of phenomena beyond the Standard Model, complementary to that achievable at the HL-LHC. For example, CLIC could provide precise measurements of the non-colored TeV-scale particles of SUSY. In particular, CLIC would enable pair-produced gaugino, slepton and heavy Higgs boson masses to be measured with $\mathcal{O}(1\%)$ precision, with sensitivity extending up to the kinematic limit of $m \approx 1.5$ TeV. In addition to studying new particles directly, CLIC provides sensitivity to New Physics through precision measurements, where, for example, Z' and Higgs compositeness models can be probed up to a scales of approximately 20 TeV and 30 TeV respectively.

Given its feasibility, staged implementation and its broad physics program beyond and complementary to HL-LHC, there is a strong case for CLIC being the next energy-frontier accelerator operating above 1 TeV. It will provide exciting research opportunities at the forefront of particle physics for several decades.

References

- [1] D. Dannheim *et al.* (editors), CLIC e^+e^- Linear Collider Studies – Input to the Snowmass Process 2013, 2013, [arXiv:1305.5766](#) 1
- [2] The European Strategy Group, Deliberation Paper on the update of the European Strategy for Particle Physics, May 7, 2013, [CERN-Council-S/103/Rev. 3](#)
- [3] CERN Council, The European Strategy for Particle Physics – Update 2013, May 7, 2013, [CERN-Council-S/106](#) 3
- [4] M. Aicheler *et al.* (editors), *A Multi-TeV Linear Collider based on CLIC Technology: CLIC Conceptual Design Report*, CERN, 2012, CERN-2012-007, JAI-2012-001, KEK Report 2012-1, PSI-12-01, SLAC-R-985, <https://edms.cern.ch/document/1234244/> 3, 4, 6, 29
- [5] L. Linssen *et al.* (editors), *Physics and Detectors at CLIC: CLIC Conceptual Design Report*, CERN, 2012, ANL-HEP-TR-12-01, CERN-2012-003, DESY 12-008, KEK Report 2011-7, [arXiv:1202.5940](#) 3, 10, 21, 23, 24, 26
- [6] P. Lebrun *et al.* (editors), *The CLIC Programme: towards a staged e^+e^- Linear Collider exploring the Terascale*, CERN, 2012, ANL-HEP-TR-12-51, CERN-2012-005, KEK Report 2012-2, MPP-2012-115, <https://edms.cern.ch/document/1234246/> 3, 6, 10, 12, 21
- [7] J. Brau *et al.* (editors), *The Physics Case for an e^+e^- Linear Collider*, 2012, [arXiv:1210.0202](#) 3
- [8] H. Aihara *et al.*, SiD Letter of Intent, 2009, [arXiv:0911.0006](#), SLAC-R-944 4
- [9] T. Abe *et al.*, *The International Large Detector: Letter of Intent*, 2010, [arXiv:1006.3396](#) 4
- [10] M. A. Thomson, Particle Flow Calorimetry and the PandoraPFA Algorithm, *Nucl. Instrum. Methods*, **A611** (2009) 25–40, [arXiv:0907.3577](#) 5
- [11] J. Marshall, A. Münnich and M. Thomson, Performance of particle flow calorimetry at CLIC, *Nucl. Instrum. Methods*, **A700** (2013) 153–162, [arXiv:1209.4039](#) 5
- [12] ILD Concept Group, *The International Large Detector Letter of Intent*, 2009, DESY-09-087 10
- [13] H. Li, Higgs recoil mass and cross-section analysis: Impacts from the ILC designs, *ILC Baseline Assesment Workshop 2*, SLAC, California, January 17–19, 2011 10
- [14] H. Baer *et al.* (editors), *The International Linear Collider TDR, Volume 2: Physics*, 2013, <http://www.linearcollider.org/ILC/Publications/Technical-Design-Report> 13
- [15] S. Dittmaier *et al.*, *Handbook of LHC Higgs Cross Sections: 2. Differential Distributions*, 2012, [arXiv:1201.3084](#) 14
- [16] F. Richard, *et al.* (editors), *TESLA Technical Design Report (part 1-6)*, 2001, [DESY-2001-011](#) 17
- [17] K. Seidel *et al.*, Top quark mass measurements at and above threshold at CLIC, 2013, [arXiv:1303.3758](#) 18, 19
- [18] P. Doublet *et al.*, Determination of Top-quark Asymmetries at the ILC, 2012, [arXiv:1202.6659](#) 20
- [19] M. A. Thomson *et al.*, The physics benchmark processes for the detector performance studies of the CLIC CDR, 2011, CERN [LCD-Note-2011-016](#) 21

- [20] B. Allanach *et al.*, The physics benchmark processes for the detector performance studies used in CLIC CDR Volume 3, 2012, CERN [LCD-Note-2012-003](#) 21
- [21] R. Contino *et al.*, Strong Higgs interactions at a linear collider, 2013, CERN-PH-TH/2013-161 23
- [22] J.-J. Blaising and J. D. Wells, Physics performances for Z' searches at 3 TeV and 1.5 TeV CLIC, (2012), [arXiv:1208.1148](#) 24
- [23] M. Battaglia and P. Ferrari, A study of $e^+e^- \rightarrow H^0 A^0 \rightarrow b\bar{b}b\bar{b}$ at 3 TeV at CLIC, 2010, CERN [LCD-Note-2010-006](#), [arXiv:1006.5659](#) 25
- [24] M. Battaglia *et al.*, Physics performances for scalar electrons, scalar muons and scalar neutrinos searches at CLIC, 2011, CERN [LCD-Note-2011-018](#) 25
- [25] L. Weuste and F. Simon, Mass and cross section measurements of light-flavored squarks at CLIC, 2011, CERN [LCD-Note-2011-027](#) 25
- [26] T. Barklow, A. Münnich and P. Roloff, Measurement of chargino and neutralino pair production at CLIC, 2011, CERN [LCD-Note-2011-037](#) 25
- [27] A. Münnich, Measurement of $\tilde{\tau}_1$ pair production at CLIC, 2012, CERN [LCD-Note-2012-004](#) 25
- [28] P. Roloff, Physics performance for measurements of chargino and neutralino pair production at a 1.4 TeV CLIC collider, 2013, CERN [LCD-Note-2012-006](#) 25
- [29] M. Battaglia *et al.*, Physics performances for scalar electron, scalar muon and scalar neutrino searches at $\sqrt{s} = 3$ TeV and 1.4 TeV at CLIC, 2012, [arXiv:1304.2825](#) 25
- [30] K. Hagiwara *et al.*, Probing the weak boson sector in $e^+e^- \rightarrow W^+W^-$, *Nucl. Phys.*, **B282** (1987) 253 27
- [31] T. Barklow *et al.*, Anomalous gauge boson couplings, *eConf*, **C960625** (1996) STC127, [arXiv:hep-ph/9611454](#) 27, 28
- [32] E. Accomando *et al.*, Physics at the CLIC multi-TeV linear collider, 2004, [hep-ph/0412251](#) 27, 28